Interfacial Slip on Rough, Patterned and Soft Surfaces: a Review of Experiments and Simulations

Thomas Lee[+,1], Eric Charrault[+] and Chiara Neto*

School of Chemistry, F11, The University of Sydney, NSW 2006, Australia

[+] These authors contributed equally to the paper.

[1] Now at the Department of Civil and Environmental Engineering, Massachusetts Institute of Technology, Cambridge, MA, 02139, USA

* Corresponding author: chiara.neto@sydney.edu.au; phone: +61-2-93512752

Table of Contents

Abstract

Advancements in the fabrication of microfluidic and nanofluidic devices and the study of liquids in confined geometries rely on understanding the boundary conditions for the flow of liquids at solid surfaces. Over the past ten years, a large number of research groups have turned to investigating flow boundary conditions, and the occurrence of interfacial slip has become increasingly well-accepted and understood. While the dependence of slip on surface wettability is fairly well understood, the effect of other surface modifications that affect surface roughness, structure and compliance, on interfacial slip is still under intense investigation. In this paper we review investigations published in the past ten years on boundary conditions for flow on complex surfaces, by which we mean rough and structured surfaces, surfaces decorated with chemical patterns, grafted with polymer layers, with adsorbed nanobubbles, and superhydrophobic surfaces. The review is divided in two interconnected parts, the first dedicated to physical experiments and the second to computational experiments on interfacial slip of simple (Newtonian) liquids on these complex surfaces. Our work is intended as an entry-level review for researchers moving into the field of interfacial slip, and as an indication of outstanding problems that need to be addressed for the field to reach full maturity.

Keywords

interfacial liquid slip, rough surfaces, structured surfaces, experiments, simulations, review

1 Introduction

Reducing energy dissipation and loss, and fabricating devices that are more efficient at no added cost are challenges that arise in every aspect of technology. These requirements are even more crucial in confined systems,[1] such as micro- and nano-fluidic devices, confined biological systems, porous materials, and thin lubricating films, where the hydrodynamic drag is very high and risks reducing the flow of liquids to zero. In these systems, being able to control the boundary conditions has a major role in driving and controlling the liquid. Understanding the boundary conditions for flow of

liquids at solid substrates is also of great importance in fluid dynamics, as it underpins the fundamental understanding of flow of liquids at interfaces.[2]

For the past two centuries one of the key concepts in fluid dynamics has been the no-slip boundary condition, i.e. the assumption that the liquid adjacent to a solid surface moves with the same velocity as the surface (

Figure 1(a)). The no-slip boundary condition was believed to be universal for simple Newtonian liquids because it was supported by macroscopic experiments over two centuries.[2-4] Up until fifteen years ago, there were only a few situations where interfacial slip was widely accepted, such as the flow of non-Newtonian complex fluids (e.g. polymer melts, polymer dispersions, micellar solutions), in liquid spreading and corner flows, and flow at gas/solid interfaces.[3]

Around the year 2000, a few experimental papers received great attention for using high-resolution techniques to prove anew the occurrence of interfacial slip in simple (Newtonian) liquids.[5-7] Thirteen years later, these observations are still controversial, but much more widely accepted. The occurrence of interfacial slip leads to a decrease in the hydrodynamic drag force acting to reduce the relative motion of a solid in a liquid, and has therefore potential implications in all systems with high surface area/volume ratio, where the relative proportion of liquid molecules that are in proximity with the solid is large. Determining the boundary condition for liquid flow over a surface requires very sensitive and accurate techniques, which have been available only in recent times, as the magnitude of any existing slip is generally expected to be small. Most measurements of slip on smooth surface have reported values of slip length in the range of a few tens of nm (see Section 2.1 for a definition of slip length).

There are however important scenarios where the slip of liquids may become evident also on a larger, macroscopic scale. Experiments on liquid flow over highly solvophobic surfaces with complex surface structure, such as superhydrophobic coatings, have found significant drag reduction on a macroscopic scale, which can be explained in terms of slip of liquids on air pockets or gas layers trapped on features of the surface. [8, 9] These experiments establish the importance of understanding boundary conditions for flow over real-world rough surfaces.

Theoretical and experimental studies on interfacial slip over the past decade have mainly focused on smooth surfaces, and aimed to establish the relationship between the surface wetting properties and the occurrence of slip. It is now commonly accepted that, on smooth surfaces, a higher magnitude of slip is obtained on non-wetting systems, [1, 3] and that slip is low or negligible on highly wettable surfaces.

Smooth surfaces (atomically smooth) are very rare in the physical world, with mica being a notable exception. Most real surfaces employed in experiments (such as solid substrates, colloid probes, channel walls and rotating disks) have a finite roughness, and surface roughness on either the micro- or nano-scale is likely to affect the interfacial flow of a liquid over a surface. Several studies have focused on the combined effect of surface wettability and surface roughness on interfacial slip. The published findings are not completely in agreement with each other, as there are many parameters that can contribute to making surface roughness act as a slip enhancer or inhibitor. Therefore at this stage no single and all-inclusive conclusion has been drawn regarding the boundary condition on rough or structured surfaces, despite numerous valid investigations.

Our aim here is to review experimental and computational studies published since the year 2000, investigating interfacial slip on *complex surfaces*, including rough and structured surfaces, surfaces

decorated with chemical patterns, superhydrophobic surfaces, and soft surfaces, i.e. grafted with polymer layers and with adsorbed nanobubbles. The need for a review on interfacial slip is strongly felt, especially in the case of complex surfaces. The field of interfacial slip is relatively novel, and, discrepancies in published results have just started to be resolved, as techniques and analysis methods are refined. The occurrence and magnitude of slip are still debated, especially in the case of complex rough and structured surfaces, where the published results are still diverse.

This review is divided into four sections: Section 2 is a brief introduction to the theory of hydrodynamic flow and the definition of a commonly used measure of slip, the slip length. Section 3 provides a few simple definitions of surface roughness. Sections 4 and 5 review, respectively, the findings of physical and computational experiments that investigate the boundary conditions at complex surfaces. We review separately the physical experiments on rough and structured surfaces, topographical and chemical patterns, surfaces with adsorbed polymers and nanobubbles, and, briefly, superhydrophobic surfaces; then we review the same topics addressed by numerical simulations. Physical and computational investigations are complementary and equally important, in that they answer slightly different aspects on the question: what boundary conditions apply on complex surfaces, and what factors determine these conditions? Finally, Section 6 provides an outlook on outstanding experimental and computational issues, and suggests approaches for evaluating the role of surface roughness and structure in determining the slip condition.

2 Background

2.1 Definition of Slip Length

The no-slip boundary condition, as illustrated schematically in

Figure 1(a), assumes that the layer of liquid next to a solid surface moves with the same velocity as the surface. The no-slip boundary condition has been demonstrated to accurately predict the flow of fluids in numerous macroscopic experiments, but has no microscopic explanation. Navier first proposed the partial slip boundary condition and introduced the idea of the "slip length", b, which is nowadays the most commonly used concept to quantify the slip of a liquid at a solid surface.[10] The slip length is the distance beyond the liquid/solid interface at which the liquid velocity linearly extrapolates to zero (Figure 1(b)). The slip length b is related to the velocity of the liquid at the solid surface v_s by the expression:

$$v_s = b\frac{\partial v}{\partial z} \qquad \textbf{(1)}$$

where v is the velocity of the fluid in the bulk and z is the axis perpendicular to the wall, as in

Figure 1.

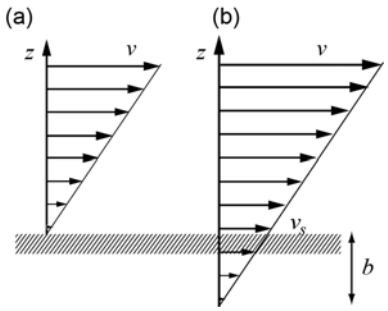

Figure 1: Schematic illustration of (a) the no-slip boundary condition, and (b) the partial slip boundary condition and the slip length b. (a) The velocity of the liquid v far from the solid surface decreases along the direction perpendicular to the wall z until it reaches zero at the stationary surface itself. (b) The velocity of the liquid decreases gradually toward the solid surface, but it is still finite v_s at the surface.

Using Navier's definition of slip length, Vinogradova derived the hydrodynamic force acting on a sphere approaching a flat surface in a liquid, including partial slip in the lubrication approximation and under the assumption of creeping flow.[11-15] This is the kind of geometry that best describes hydrodynamic measurements performed by colloid probe atomic force microscopy (CP-AFM) and surface forces apparatus (SFA). The hydrodynamic force on a sphere approaching a flat surface is

$$F = \frac{6\pi\eta R^2 v}{h} f^* \qquad \textbf{(2)}$$

where η is the viscosity of the liquid, R is the radius of the microsphere, v is the velocity of the microsphere relative and perpendicular to the substrate, h is the distance of closest approach of the sphere surface to the substrate surface, and the correction factor f^* accounts for the occurrence of interfacial slip. Assuming the same slip length b at both surfaces, f^* is:

$$f^* = \frac{h}{3b}\left[\left(1+\frac{h}{3b}\right)\ln\left(1+\frac{6b}{h}\right)-1\right] \qquad \textbf{(3)}$$

The correction factor f^*only depends on the slip length b and on the surface separation h. The factor f^* can be smaller or equal to 1. For $f^* = 1$, the no-slip hydrodynamic force is recovered.[6] In case of interfacial slip, $f^* < 1$, and the effect of slip is to reduce the hydrodynamic force exerted on a sphere approaching a flat surface, that is, slip increases the rate of drainage of the liquid confined between two surfaces being driven together with a constant force.

2.2 Experimental Techniques Employed to Investigate Boundary Conditions

Recent reviews provide a detailed description of the techniques that have been employed to investigate boundary conditions for flow, so we will not review them here.[3, 16-18]. Briefly, these techniques can be classified as either direct, for which the flow of tracer molecules or particles is observed to deduce the flow of the liquid directly, or indirect techniques, for which a physical quantity is measured and a slip length value is fitted using existing theories, such as in hydrodynamic force experiments.

Among the direct techniques, the most commonly employed are micro-particle image velocimetry (μ-PIV) [19, 20], and total internal reflection fluorescence (TIRF) [5]. Many recent improvements have enhanced the resolution on the determination of the velocity at the wall for such optical methods.[21-23] Recent μ-PIV experiments making use of evanescent waves and nanoscaled particles enhance the resolution to 10 nm.[22] Bolognesi *et al.* reported the development of a new μ-PIV set-up which measures simultaneously the velocity field and the profile of a liquid meniscus with a resolution of a few tens of nanometers, by digital processing images of a liquid seeded with fluorescent passive tracers.[24]

Among the indirect techniques, slip lengths can be obtained via the measurement of hydrodynamic forces with the colloid probe atomic force microscope (CP-AFM) [6] or surface force apparatus

(SFA);[25, 26] other common indirect methods include torque measurements with a rheometer, [27], and pressure drop analysis,[28] where pressure and flow rate are usually measured in a channel.

An important aspect when comparing results (even on smooth surfaces) obtained by different techniques is resolution. The colloid probe colloid probe (CP-AFM) is among the most accurate techniques to measure interfacial slip, with a resolution on surface separation of 1-2 nm. The Neto group recently contributed to greatly improving the reliability and reproducibility of slip results obtained with colloid probe atomic force microscopy, reaching a resolution on the measurement of slip length of the order of 5 nm.[29-32] Other techniques, such as those probing flow through micro-channels or between rotating plates, work at a much larger scale, without any high confinement effect, and the generally associated measurement techniques (fluorescence recovery after photobleaching, FRAP, or particle imaging velocimetry, PIV) have a lower resolution on the slip length of around 50 nm.[4, 44] This difference in resolution determines largely the difference in conclusions that can be drawn from results obtained with these techniques.

2.3 Definition of Reference Surface

One of the most important issues when defining interfacial slip on complex (rough and structured) surfaces is the uncertainty on the location of the "reference surface", i.e. the line from which the slip velocity is determined. The choice of the reference surface greatly affects the interpretation of most experiments, and can have major repercussions on the magnitude of the reported slip length. The different choices of reference surface are illustrated in Figure 2. For a smooth substrate, the reference surface is unambiguous and coincides with the solid surface. For a rough or structured substrate, the reference surface may be defined to coincide either with the peaks of the roughness features (part (a)) and of the fabricated features (part (b)), or the bottom of the roughness valleys/features, or somewhere in between these two.

Due to their geometries, most techniques impose the location of this reference surface. In CP-AFM experiments, the colloid probe is made to approach a flat substrate and the "zero of separation" (needed to analyze the force curves) is when the two highest features on the opposing surfaces enter in hard contact, so the reference surface is necessarily located at the peaks of the roughness. In traditional SFA experiments, where mica is used as a substrate, the zero of separation is usually defined when the two smooth opposing mica surfaces are in contact in air. Surface features added afterwards to confer roughness or structure are therefore located above the reference surface. Although a hydrodynamic drainage force model is required to estimate the slip with these techniques, the different locations of the reference surface result in different (and controversial) slip length values. Other methods are based on average quantities, such as pressure or fluorescence recovery measurements. In these cases, a defined volume element is probed from the wall, no matter if the wall is rough or smooth, imposing the reference surface as the bottom of the surface elements.

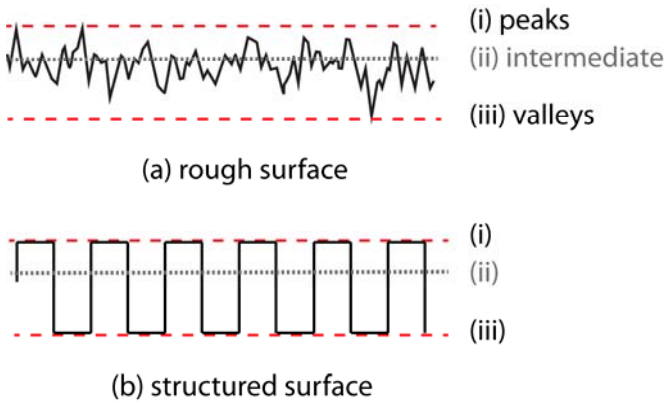

Figure 2: Three different choices of reference surface to establish interfacial slip for (a) rough surfaces, and (b) structured surfaces containing fabricated pillars.

2.4 Laminar Flows in Newtonian Liquids

This review focuses on the boundary conditions of flow of Newtonian liquids. Liquids are defined as Newtonian when their behavior is purely viscous. This means that their viscosity depends uniquely on temperature and not on shear rate, up to very high values of the shear rate.[33] From a molecular point of view, Newtonian liquids are made of low molecular weight molecules, such as water and most low molecular weight organic solvents. Non-Newtonian liquids include a wide category of liquids, such as polymer melts, polymer dispersions, and micellar solutions, whose viscosity depends critically on the shear rate.

In this review we focus our attention on laminar flow, under which the liquid molecules flow in undisturbed parallel layers. We are concerned with the flow of liquids at low Reynolds numbers (R_e< 1), $R_e = \rho v l / \eta$, where ρ and η are the density and viscosity of the liquid respectively, v is the rate of the liquid flow and l is the characteristic length scale of the flow. In most macroscopic systems the Reynolds number is considerably larger than 1 and the flow is turbulent. In colloidal systems or when the flow is confined, $R_e < 1$ as a consequence of a small characteristic length scale of the flow. In this cases the flow is laminar, and experiments in this regime are easier to understand and model.[3]

2.5 Intrinsic and Effective Slip

In physical experimental studies of the boundary condition, there is an unavoidable uncertainty in the nanoscopic details of the liquid/solid interface, including aspects such as trace chemical or particulate contamination, depleted solvent layers, nano-scale roughness, or trapped air in the form of nanobubbles.[3, 34] In practice, in experiments, measurements of the "intrinsic" slip length, i.e. the slip length that would be measured if the interface was atomically flat and homogeneous with no local change in viscosity, is impossible. What is measured and reported is the "effective" slip length, which can adequately describe flows and hydrodynamic forces farther from the interface, beyond the first few molecular layers of liquid. We will denote the effective slip length b_{eff}. Although the intrinsic slip length is of fundamental interest, in many practical cases the effective slip length is extremely useful in describing and understanding microfluidic systems. In such situations specific knowledge of the details of the fluid motion within a few nanometers of the interface may not be required.

Computational studies using molecular dynamics are capable of investigating and measuring intrinsic slip at the surface, and have in many cases shown that the intrinsic slip increases as the strength of the attraction between fluid and solid is decreased.[35, 36] In such molecular dynamics

simulations the main challenge is to choose interatomic potentials that are realistic enough to describe the physics of the flow, while still being computationally efficient. Other simulation details are also important, such as the thermostatting procedure.[37, 38]

Similar considerations apply in the case of a surface with topographical or chemical patterns; here the fluid flow near the interface can be highly complex, even resembling eddies and vortices normally only observed in turbulent flow.[39-41] Farther from such an interface, at a distance on the order of the lateral length scale of the inhomogeneities, these chaotic motions dissipate, and the flow begins to resemble that which might occur over a flat unpatterned surface.[42, 43] Again the concept of an effective slip length can be of value in these cases. For nanoscale patterns, as stated above, physical experiments will in general probe the flow in the region far from the patterned surface (farther than a distance of the order of the pattern length scale) and allow an effective slip length to be measured (see Section 4 for a discussion of the length scales probed by experiments). While simulations can resolve the complex microscopic flow near a patterned interface if required,[39-41] the effective slip length relative to an appropriate reference surface is still of interest in order to make real world comparisons and predictions, and as a convenient way of quantifying the extent to which a rough, patterned, or soft matter interface enhances or inhibits fluid flow.

3 Definition of Surface Roughness

Several parameters can be used to define surface roughness. The most commonly used are the peak-to valley roughness (r_{max}), the average roughness (r_a), and the root mean squared roughness (r_q). [44] The value of r_{max} is defined as the difference between the highest value of vertical position on the surface, i.e. the peak (z_{max}), and the lowest value of vertical position on the surface, the valley (z_{min}), as indicated by $r_{max} = z_{max} - z_{min}$. The value of r_{max} changes drastically whenever even just a few high protrusions and deep scratches are present on the surface. The value of r_a is calculated as the average absolute deviation of all the vertical positions on the surface from the mean line over a sampling length l. The value of r_a gives a good average description of the height variations on the surface: $r_a = \frac{1}{l}\int_0^l |z(x)|\,dx$. The mean line is determined by equating the area enclosed by the profile of the surface above and below the line. The value of r_q is given by the standard deviation of the surface heights distribution, and is more sensitive than r_a to large deviations from the mean line: $r_q = \sqrt{\frac{1}{l}\int_0^l z(x)^2\,dx}$.

Roughness undoubtedly alters the behavior of a liquid flowing over a surface, as the contacting solid surface exhibits variations in the number of interacting surface atoms. It is reasonable to assume that on one hand the surface high peaks add resistance to the flow, and that on the other hand the surface cavities/valleys offer a better drainage of the liquid. Most real world surfaces have a finite surface roughness which depends on the surface preparation process. Only mica can be cleaved into large (cm-size) areas that are atomically smooth.[45] Silicon wafers are commonly considered very smooth surfaces, but they exhibit a small and finite roughness (r_q can be as low as 0.2 nm). Most real surfaces possess a finite surface roughness.

In the following we have chosen to call “rough” surfaces on which roughness has been induced by self-assembly methods, mechanical polishing or grinding, chemical etching or adsorption of entities on the surface, such as particles or polymers (a random roughness such as depicted in Figure 2(a)). We will call “structured” surfaces on which the features have been explicitly fabricated by the user,

as for example in structures formed by photolithography, or by deposition of nanoparticles that are specifically engineered to modify the properties of the surface (Figure 2(b)).

4 Physical Experiments on Interfacial Slip

Before moving to describing issues concerning the slip on complex surfaces, we will briefly address issues that affect all slip investigations, including those on smooth surfaces. Several techniques have been used to measure interfacial slip on smooth surfaces, including those listed in Section 2.2, all with different resolution.[3] Each technique, due to its geometry and method of operation, offers different observations of the flow boundary conditions. As an example, let's consider the hydrodynamic drainage forces measured with both CP-AFM and the SFA. The typical radius of the probes mounted in these two techniques varies by several orders of magnitude, being respectively $R_{AFM} \approx 10$ μm and $R_{SFA} \approx 2$ cm. The resulting studied area is therefore much larger in the case of an SFA experiment where an estimated contact diameter is approximately 10 μm, compared to the approximately 10 nm in a CP-AFM (under the force of about 1 nN, with no adhesion between the contacting surfaces).

More generally, the lateral distance on the surface being probed during a hydrodynamic experiment is of the order $\sqrt{2Rh}$ [24, 46, 47], where R is the radius of the probe and h is the distance of closest separation between the probe and the surface. When the two surfaces are in contact, $\sqrt{2Rh}$ is approximately the diameter of the contact area and when the two surfaces are far away $\sqrt{2Rh}$ coincides with the diameter of the probe. Even though the effects of the boundary condition can be felt in a region outside the actual contact area, it is clear that when studying the effect of roughness on the slip properties of a heterogeneous surface, great care is required to relate roughness length scale to the technique. This aspect is illustrated in Figure 3. The roughness illustrated in part (a) and part (b) can be probed by the AFM colloid probe, and the investigated flow conditions will be an average of the whole structured area under the probe. Conversely, the length scale of the structure in part (c) is of the same order of magnitude as that of the probe diameter, and so this roughness cannot be reliably tested by AFM.

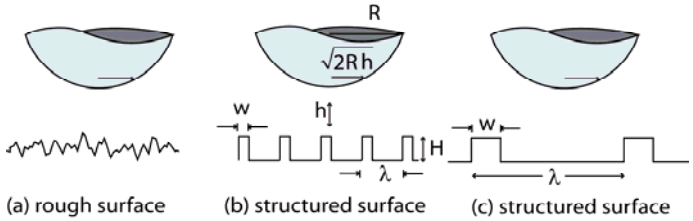

Figure 3: Schematic illustration of an AFM colloid probe approaching (a) a rough surface, (b) a structure surfaced with pillars, whose surface density is large compared to the size of the colloid probe, and (c) a structured surface with relatively large and sparse features. The value of $\sqrt{2Rh}$ estimates the lateral length probed during the approach. Other parameters defined here are the radius of the colloid probe (R) and probe-surface distance of closest separation (h); parameters of the structure are defined here: width (w) of the features, pitch (λ), and height of the features (H).

A more subtle experimental aspect that is often overlooked is the possible interference of phenomena that occur at the nanoscale in the liquid as a consequence of the experimental design. For example, liquid molecules confined in the thin liquid film between approaching flat mica surfaces in an SFA experiment may become ordered in molecular layers at low rates. [48] It has been demonstrated that the orientation of the mica lattices greatly affects the friction of the confined film and therefore slip.

[49] In AFM the confinement effect is much reduced, but it is still possible to observe solvation forces due to the presence of single asperities protruding from the surface of the microsphere. [50]

These issues are further complicated by the addition of surface roughness or structure. The interpretation of results acquired on rough and structured surfaces is complicated by the uncertainty in the wall position that is associated with roughness, as mentioned in Section 2.3. This effectively reduces the resolution of even highly accurate techniques such as AFM. In practice, slip and no-slip boundary conditions cannot be distinguished on rough surfaces in situations where the measured slip length is of the same order as the typical peak-to-valley roughness of the surface.

4.1 Slip on Rough Surfaces

It is intuitive that boundary slip should be affected by surface roughness,[3, 26, 51, 52] but so far discrepancies in the magnitude of measured slip between published physical experiments have made it hard to draw a simple picture. Results of simulations in this respect are clearer cut and can help in directing experimental investigation (see Section 5). Relatively few experimental studies have concentrated on investigating solely the influence of roughness on boundary slip. These experiments are challenging for a number of reasons, as detailed below in Sections 4.1.1 to 4.1.3: (i) it is difficult to produce suitable surfaces of controlled roughness, without producing undesired changes to other interface properties, such as wettability. This makes it hard to decouple the individual effects of roughness and wettability on slip. (ii) Nanoscale and microscale roughness could clearly have different effects on slip. An appropriate and complete theoretical description of realistic surface roughness is yet to be found. (iii) The position of the reference surface in drainage force experiments is ambiguous, and slip could be replaced by the idea of a “shifted boundary”.

4.1.1 Link between Roughness and Wettability

Most surface modification methods designed to alter specifically surface roughness inevitably alter wettability as well. In general terms, surface roughness magnifies the intrinsic wetting properties of a surface, enhancing both the solvophilicity or solvophobicity of a surface.[53]. The main effect of surface roughness on contact angle is described by the Wenzel equation and the Cassie-Baxter equation.[54, 55] Two limiting behaviors are described according to these models, and these are summarized in Figure 4. In Figure 4(a) a droplet of liquid is placed on a structured surface: in this case, the liquid can penetrate into the holes in the structure and is therefore in contact with the surface at every point within its footprint. The situation in part (a) is often described as the Wenzel regime. In Figure 4(b) the features of the structure are such that they trap air pockets within their holes, so that the droplet only contacts selected regions of the structures, namely the tops of the pillars. The situation in this case is described as the Cassie regime. In practice, the liquid often penetrates within the surface crevices, producing a Wenzel regime, even if the contact angle of the liquid on the surface is greater than 90 degrees, as the trapping of air in the crevices is thermodynamically unfavored.[56] We encounter these two regimes and their potential influence on interfacial slip in Section 4.2.3.

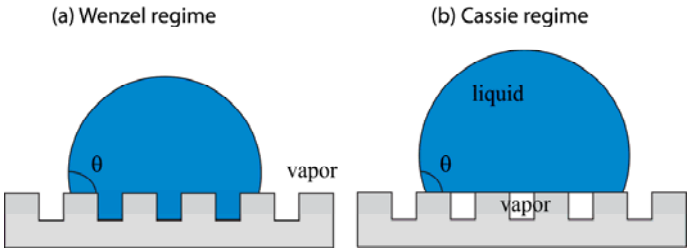

Figure 4: Schematic illustration of a droplet over a structured surface. (a) In the Wenzel regime a liquid droplet placed on top of a rough or structured surface completely wets the surface, entirely filling the crevices present of the surface. (b) In the Cassie-Baxter regime, the liquid sits on top of the crevices, and air pockets can be trapped within the crevices of the surface.

4.1.2 Nanoscale versus Microscale Roughness

The effect of both nanoscale and microscale roughness on slip has been investigated. Combining a rotating plate technique and TIR-FRAP, the Léger group showed that on a rough and incomplete fluorinated SAM layer on sapphire, slip was inhibited by the presence of heterogeneities at the molecular level.[5] On a roughness created by depositing PS nanoparticles on a rotating sapphire plate, they found that increasing the height of the corrugations inhibited the slip, whereas increasing their width enhanced it.[57] In this case the intrinsic roughness of the sapphire surfaces, which presented multiple nano-scratches, was not taken into account.

On the microscale roughness front, on a poorly wettable polymer surface, Ligrani *et al.* used a rotating-disk and pressure-slip flow model to measure an increase of the slip length with the average size of the roughness (b up to 1.7 μm for a disk with r_q = 707 nm).[58] They defined the reference surface at the peaks of the surface elements.

Experiments measuring pressure drops in micro-channels showed that increasing the roughness of the wall led to a no-slip boundary condition and also resulted in an early laminar to turbulent transition.[59-61] Some results obtained by QCM experiments have been contradicting: a rough crystal surface was found to suppress slip of Newtonian wetting liquids,[62] while in a similar situation slip was found to be present, and to increase with increasing shear rate and with increasing viscosity of the liquid.[63]

4.1.3 Effect of Shifted Boundary

The issue of surface roughness (and surface structure) is particularly hard to address in experiments where hydrodynamic forces are used to derive the slip length, such as those obtained by colloid probe AFM and SFA. A different choice of reference surface can lead to a shift of the force curve and as a consequence a different value of the slip length, as pointed out by the Vinogradova and Craig groups.[64, 65] Indeed if the hard contact between approaching rough surfaces is set to occur at the top of the peaks, the measured effective slip will tend to be larger as the liquid molecules can still flow at the bottom of the valleys.

Consider the case of a rough surface at which a no-slip boundary condition applies. As fluid is sheared over such a surface, the flow-lines will appear complex near the surface due to the requirement that the fluid navigate around the asperities.[37, 38] A flat surface could be placed at the highest points of the roughness, and a Navier slip boundary condition could be assumed at this hypothetical surface, and experimental or computational observations fitted to obtain an effective slip length, as is done when studying flat surfaces. However it has been suggested that this effective slip model is incorrect,[59, 61, 110] and that the flow over such an interface is better described by considering a hypothetical smooth surface at which a no-slip boundary condition applies, shifted a

distance s below the top of the roughness. The value of s can be obtained by fitting experimental or computational results. This treatment is called a "shifted boundary" model to distinguish it from the Navier slip model.

Performing hydrodynamic drainage experiment with CP-AFM on a rough surface (r_{max} < 45 nm), Vinogradova *et al.* were the first to point out that in case of a poorly wetting interface, although a slip length of 48 nm could fit the experimental force curve at large separations, a good fit was achieved both at large and small separations by considering a no-slip boundary condition on a reference surface shifted by a distance s = 45 nm into the rough surface.[64] This result is illustrated in Figure 5(a). The drainage force in the shifted boundary case differs from that of the Navier slip case by a factor of $h/[(h+s)f^*]$, where h is the sphere-plane separation and f^* is the factor defined in Section 2.1.[64] Because the separation changes throughout the experiment, a single force curve is sufficient to distinguish between the two models. At large separations, the difference $h/[(h+s)f^*] \approx 1$, but at small separations the shifted surface model will result in a lower force than predicted by the Navier slip model. Simulated lattice Boltzmann colloid probe experiments[66] and CP-AFM experiments[64] both support the fitting of an effective no-slip boundary condition, demonstrating significantly better fit to the forces at small separation. The simulation result is shown in Figure 5(b), and compared to no-slip, Navier slip, and shifted surface models, the latter of which clearly provides the better fit at small separations.

Another possible way to estimate the hydrodynamic force on rough surfaces is to find reasonable lower and upper boundaries. The measured force should lie below the force between a smooth surface placed at the top of the roughness peaks and above the force expected if a smooth surface is placed at the bottom of the roughness valley.[52, 65] In general, it is crucial to compare the measured slip values with the size of the roughness. Similar values might indicate that a no-slip theory could be applicable by shifting the contact line "inside" the roughness.[64-66]. A position within the roughness near the r_a value of the surface would be then a more reasonable choice. The concept of shifted boundary is also discussed in Section 5.1.1.

The Craig group measured large slip lengths on rough silica (b up to 900 nm, r_{max} = 50 nm) using CP-AFM and represent one of the rare cases where the slip is much greater than the roughness of the surface.[52] Later, and following the concept of the shifted boundary, they studied the same system and concluded that a no-slip boundary condition was required for hydrophilic surfaces, and discrepancies could be explained with the use of V-shaped cantilevers.[65] The effect of cantilever type was also discussed elsewhere.[67, 68] The Neto group has shown that the slip length measured by CP-AFM can be overestimated, and a spurious dependence on cantilever shape and drive velocity observed, if the contribution of the hydrodynamic drag on the (soft) cantilever is assumed to be constant. For soft AFM cantilevers, a complete calculation of the non-constant drag force on the cantilever is necessary, and eliminates any effect of cantilever shape and drive velocity.[30]

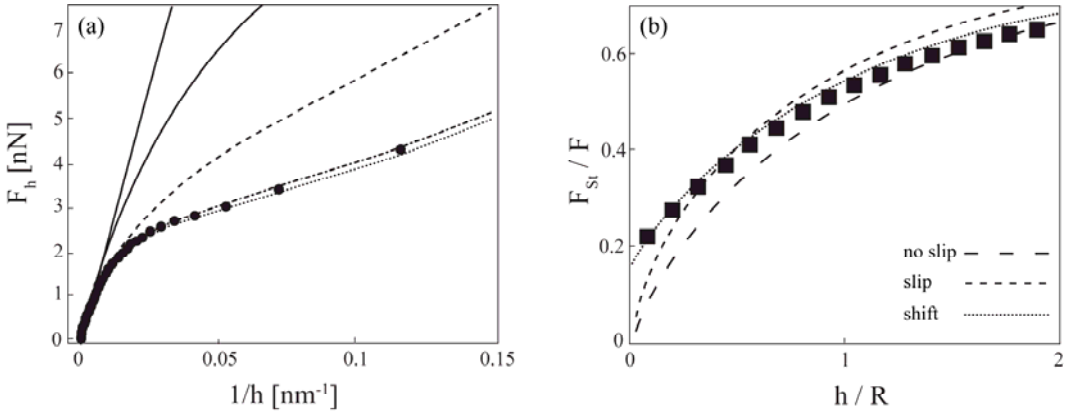

Figure 5: (a) Hydrodynamic force as a function of the inverse of separation (●). The solid line represents the no-slip boundary condition. The dashed curve shows the slip boundary condition (b = 48 nm) and the dotted curve corresponds to a no-slip boundary condition shifted by s = 48 nm into the rough surface. The best fit is obtained for s = 45 nm (dashed-dotted line). Adapted from Vinogradova *et al.* [64] with permission. (b) Simulated colloid probe force-distance curve (■) using the lattice Boltzmann method, expressed as inverse normalized force ($F_{St} = 6\pi\mu Rv$) as a function of normalized distance. The dashed lines represent fits to no-slip, Navier slip, and shifted surface models. Adapted from reference [66] with permission.

4.2 Slip on Structured Surfaces

The consequences of structuring a surface on its behavior with respect to liquid flow are highlighted by nature's most famous example of slippery surface, the lotus leaf.[69] Its particular hierarchical roughness at the micro- and sub-micrometer scale gives the lotus leaf extreme water-repellent properties and makes water droplets roll over it, due to the trapping of interfacial air under the droplet.[70] Over the past decade the boundary conditions of flow over structured superhydrophobic surfaces have been intensively investigated,[9, 28, 71-79] as part of an effort to design surfaces mimicking the topography and water repellence of the lotus leaf and other biologically inspired surfaces.[46, 80, 81] Slip lengths of large magnitude have been measured on such surfaces, up to a few micrometers, [74-76, 82] and as a consequence there is growing interest in engineered structured surfaces to reach even larger slip lengths. There seems to be unanimous agreement that the large interfacial slip measured on superhydrophobic surfaces is due to the presence of air bubbles or air layers trapped within the structures. However, results regarding wetting structured interfaces are more controversial and often in disagreement with each other. Although slip has also been measured over wetting interfaces,[68, 82, 83] it has been claimed that a shift of the no-slip reference surface inside the structured surface could describe the hydrodynamics of such surfaces, similarly to the case of rough surfaces described in Section 4.1.[84]

4.2.1 Fabrication of Surface Structures

A number of complex surfaces with sophisticated surface chemistry and topography have been developed to control and enhance the wetting properties of surfaces, with the aim to fabricate surfaces with huge slip, enabling a brand new branch in the microfluidic research field. Structured surfaces possess a type of engineered well-defined roughness, typically at larger (micron) scale than rough surfaces. The fabrication of engineered structure on a surface is very useful in studies of liquid flow at interfaces, as it allows determining the influence of length scale of well-defined structures on slip. Various geometries have been fabricated in order to study interfacial flow on structured surfaces, as depicted in Figure 6. The most commonly studied geometries are pillars,[46, 74, 82] grooves and ridges,[20, 68, 74, 84] and most recently holes.[85-87] These structures are defined by

their width (w), height (H), and period or pitch (λ), as depicted in Figure 3. Various kinds of grooves or riblets (saw tooth, scalloped or blade) are common in mimicking sharkskin and are mostly investigated in relation to reducing drag in turbulent flow.[88, 89]

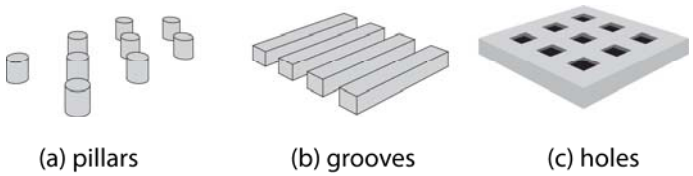

Figure 6: Common geometries used in experimental and numerical studies on interfacial slip on structured surfaces.

Various methods have been used to develop structures on surfaces. We do not intend to review fabrication processes here, but will provide a few illustrative examples. Several types of lithography are commonly used to achieve the desired structures, such as photolithography,[83] etching,[83, 86, 87] focused ion beam,[68] and micromolding.[20] Once the structures have been fabricated, the surface typically needs to be chemically treated to obtain specific wettability properties. The interest in superhydrophobic surfaces has resulted in the use of numerous coatings that lower the surface energy, including alkyl- or fluoro-silanes, and hydrophobic polymers such as PTFE.

4.2.2 Slip on Wetting Structured Surfaces

As a consequence of the growing interest in superhydrophobic surfaces, few studies have focused on investigating interfacial slip on wetting structured surfaces. A few recent studies are summarized here. Using hydrodynamic force experiments with CP-AFM, Guriyanova *et al.* showed that in a partially wetting system, the degree of slip slightly increased when the surface was structured (grooves with H = 20 nm and λ = 500 nm), and that slip was further enhanced by superimposing an irregular roughness (Figure 7).[68] They also demonstrated that regardless of the wettability of the surface, the measured slip lengths exceeded the peak-to-valley roughness (H) of their surface features and were smaller than the shift distances required to recover the no-slip boundary condition at an imaginary surface. Consequently, they concluded that a true effective slip was present.

Using an original apparatus using gravity to displace a macroscopic sphere towards a grooves structured surface ($\lambda \approx 200$ µm, $w \approx 100$ µm, $H \approx 45$ µm), Mongruel *et al.* observed drag reduction due to the presence of the structures and that this reduction increased with increasing ratio λ/w.[84] They showed that their results could be described by a no-slip boundary condition applied at an imaginary smooth surface located between the top and bottom of the corrugations.

Drag force reductions were observed using SFA by Gupta *et al.* on a surface structured with hexagonal arrays of micrometric pillars.[46] By modifying a scaling analysis from Persson, they established a characteristic distance of closest separation h_0, below which the liquid can penetrate the space between the pillars. This characteristic separation was found to be linearly proportional to the separation at which no-slip and slip hydrodynamic theory diverge. Yamada *et al.* showed that the rib structuration of a channel, regardless of its wettability, results in a reduction of the friction factor compared to a smooth channel.[83]

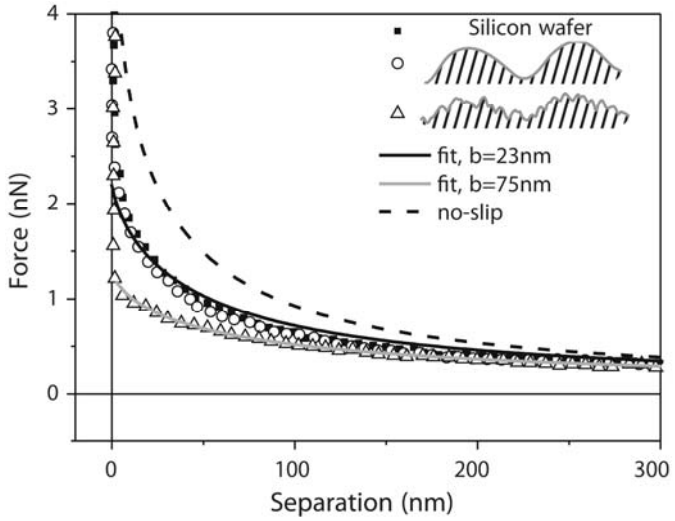

Figure 7: Hydrodynamic force curves measured in approach between a colloid probe and three surfaces (flat silicon wafer ●, structured surface ○ and, hierarchical surface △). Lines represent the calculated curves corresponding to a no-slip boundary condition (dashed), and a slip boundary condition with b = 23 nm (black) and b = 75 nm (grey). Adapted from Guriyanova *et al.* [68] with permission.

4.2.3 Slip on Superhydrophobic Surfaces

Investigations of interfacial slip on superhydrophobic surfaces have recently been reviewed.[82, 90-92]. Superhydrophobic surfaces are of great interest since they often result in a large degree of drag reduction and friction factor reduction, which could improve the flow and transport in the liquid phase in devices operating at the micro- and nanoscales. Studies on the macroscopic scale have also measured a drag reduction, for example in fully immersed surfaces. Dong *et al.* structured the surface of a macroscopic model ship to make it water repellent and measured an increase of drag reduction at large velocities.[8] They related their results to the presence of an air layer that was retained by the immersed surface (plastron effect), hence proving that the air-water interface entrapped on the surface structures was efficient at a macroscopic level.

Slip over various non-wetting and structured surfaces in a Cassie regime has been investigated with both direct and indirect techniques for various structure geometries. It has been widely accepted that air bubbles entrapped on surface structures are the cause of the high degree of interfacial slip and low drag measured experimentally because of they are a "shear-free boundary".[28, 77] The general observation is that interfacial slip increases with both the air fraction and the pitch of the structure, as long as the interface remains in a dewetted Cassie state (as depicted in Figure 4(b)). In this regime it is common to obtain values of slip length of up to several micrometers. [27, 78, 93-95] The apparent air fraction at the solid/liquid interface, together with the shape of the air protrusion, are both parameters strongly affecting the degree interfacial slip (see also Section 5.2.2).[85]

Using CP-AFM, Maali *et al.* investigated slip on a surface structured with pillars, which led to surfaces in both the Wenzel regime and the Cassie regime.[96] While no slip length was extracted in the Wenzel regime, the authors measured slip in the Cassie regime, and fitted different values of the slip length on top of pillars ($b_{\text{local-pillar}}$ = 119 nm) and in the region between pillars ($b_{\text{local-pillar}}$ =356 nm). Joseph *et al.* used micro-PIV to study the effect of a surface structured with carbon nanotubes.[97] They observed a no-slip boundary condition on a surface in a Wenzel state and interfacial slip of the order of one micrometer on surfaces in the Cassie state. The magnitude of the slip was shown to increase with the lateral roughness scale. Studying the liquid flow on a porous hydrophobic coated pipe, Watanabe *et al.* measured a reduction of the drag flow and interfacial slip,

and concluded that liquid slip occurred because of air entrapped in fine grooves present at the surface of the wall after coating.[98] Ou *et al.* used a pressure drop experiment [77] and a micro-PIV [28] to demonstrate that the presence of an air-water interface led to high slip lengths (20 μm) and that the pressure drop reduction increased for well-defined feature size (small channel depth combined with large spacing).

Looking at liquid flow over polydimethylsiloxane grooves, Tsai et al showed that the effective interfacial slip length increases linearly with the ratio w/h.[20] They observed that the local interfacial slip length was higher on porous grooves than on smooth ones. Their results are in agreement (although lower) with the theoretical work of Philip,[99] which predicted the same behavior when a liquid is flowing over a smooth surface patterned with contiguous no-slip and shear-free domains. The measure of the longitudinal and transverse flow velocities at a level located inside the groove highlighted the effect of the meniscus shape on the interfacial slip. Byun *et al.* showed that due to the penetration of the liquid into the cavity to form a convex meniscus on grooves, interfacial slip increased when the ratio w/λ decreased.[100]

The Kim group showed that large slip lengths (up to several hundred micrometers) can be measured on microstructured,[74] nanostructured [27] and hierarchical surfaces, [75, 76] at low values of solid fraction (hence for large amount of air entrapped within the structures). They demonstrated that as the gas fraction increases by increasing the pitch, a transition from a Cassie towards a Wenzel state could occur and lead to a decrease of the interfacial slip. They pointed out that this transition can be delayed to higher pitch values by adding nanostructures on the side of the microstructures.[76] In a following paper, as illustrated in Figure 8, they showed that adding the nanostructures on top of pillars increased the interfacial slip compared to smooth pillar only if the surface solid fraction Φ_{micro} (defined by the microstructures) was above about 10%.[75] Below this value, the opposite effect was observed with a decrease of the interfacial slip on the hierarchical surface. This effect is highlighted Figure 8 by the dotted line separating the two regimes. They discussed their results arguing that as long as the liquid pressure was sustained by the microstructures (three phase contact line on top of the microstructure and microstructures not participating in resisting the liquid pressure), the secondary structure enhanced the interfacial slip. This was supported by some numerical studies that showed a decrease of the interfacial slip when the three phase contact line slides along the microstructures.[101]

Using dynamic damping AFM experiments, Bhushan *et al.* calculated the total damping coefficient via the measure of the amplitude and phase shift as the cantilever oscillated while approaching the surface.[102] They showed that the hydrodynamic damping coefficient decreased on poorly-wettable surfaces, with the lowest coefficient being observed for a structured superhydrophobic surface (tubules). The values of slip length measured were around twice the size of the structures. Recently, Busse *et al.* revisited analytically the theoretical predictions for an ideal superhydrophobic surface possessing a constant gas layer thickness in spite of the flow.[103] They pointed out that the classical lubrication equations overestimated the effective slip length and drag reduction for various systems.

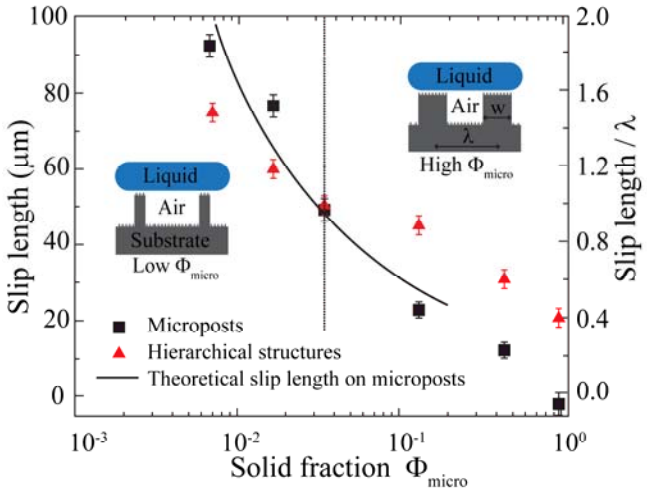

Figure 8: The effect of nanoposts added on top of microposts on the overall slip. The measured slip lengths on smooth (■) and rough (▲) microposts are depicted along with the theoretical slip length prediction on posts (curve) versus surface fraction occupied by microstructures. Schematics of the high and low solid fractions are also represented. Adapted from Lee *et al.* [75] with permission.

4.3 Slip on Surfaces Bearing Nano-bubbles

The ability to produce nanobubbles on hydrophobic surfaces in a controlled fashion by the solvent exchange method has opened up new opportunities for investigation for interfacial slip at liquid/vapor interfaces.[104-107]. Interestingly, the presence of embedded air bubbles on a surface does not always result in a lower drag. It has been shown (

Figure 9) that rather than the fraction of air/liquid interface, it is the shape of the meniscus at the gas interface that mainly affects the interfacial slip, and that the maximum magnitude of slip is obtained for a zero angle. [85, 87] On a surface structured with holes, a larger effective slip length was measured on a hydrophilic Wenzel interface than on a hydrophobic Cassie interface. The ability to tune the shape of the liquid-gas interface, thus to create "air-structured" surfaces seems to be an efficient way to control the interfacial slip. Kashninejad *et al.* [86] showed that wider holes resulted in higher velocity increase and higher slip length. Also, by studying the eccentricity of the holes, they demonstrated that the slip length is higher for structured surfaces that exhibit a low contact angle hysteresis.

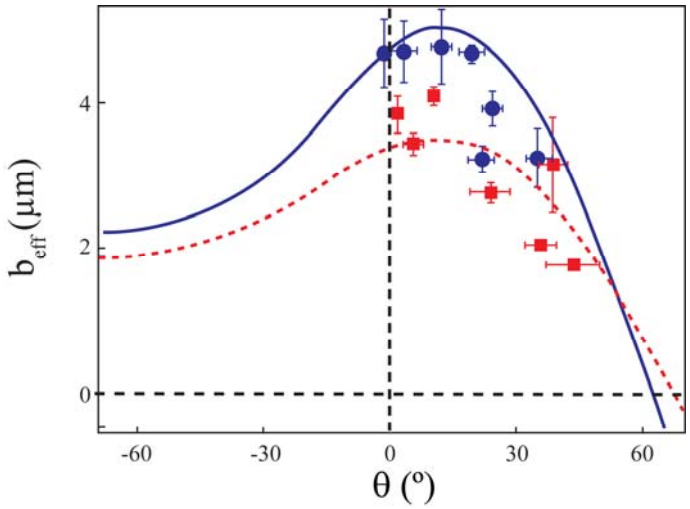

Figure 9: Evolution of the effective experimental (■) and numerical (●) slip length with the protrusion angle θ on a hydrophobic "bubble mattress". Adapted from Karatay *et al.* [85] with permission.

4.4 Slip on Chemical Patterns

It can be argued that the flow of liquids over superhydrophobic surfaces in the Cassie state is indeed a flow over a chemical pattern, as it occurs over patches of air alternating with patches of solid surface. Here we focus specifically on slip investigations on surfaces where the chemistry has been patterned on a microscale with monolayers or thin layers. This topic has not really been addressed in physical experiments, while there are several numerical simulations dedicated to studying the boundary conditions for the flow of liquids on surfaces patterned with domains of distinct chemistry, as described in Section 5.2.1. However experiments have been conducted in open microfluidic systems, such as channels formed by hydrophilic stripes on a hydrophobic background. These studies enable the study of a liquid flowing at two different interfaces (air and solid). Using an open microfluidic system, Yang *et al.* measured the motion of a liquid front driven by capillary forces in a hydrophilic channel within a hydrophobic matrix.[108] Their results are in good agreement with the Washburn theory using a no-slip boundary condition at the air-water interface. Using a similar open channel technique, Zheng at al. showed that a partial slip, instead of a stress free boundary, describes more accurately the boundary condition of the air-water interface.[109] In their study, Kim *et al.* claimed that the air-water interface seems to behave like a no-slip interface and that the structuration of a fully wetting interface results in less friction that that of a non-wetting one (Cassie).[110]

4.5 Slip on Grafted Polymer Brushes

Compared to rigid surfaces, considerably little attention has been directed towards characterization of flow over surfaces composed of soft matter. An often studied example of a synthetic soft matter surface is a polymer brush – a surface composed of polymer chains end-grafted onto a solid substrate, which when exposed to a good solvent becomes swollen causing the chains to stretch away from the surface.[111]. In addition to a vast number of possible chemical functionalities, polymer brush surfaces have the potential to reversibly switch their properties and structure in reaction to changes in their environment (for example solvent quality, temperature, salt concentration), with potential application in responsive components for microfluidic devices.[112] The hydrodynamics of flows over soft surfaces is of interest for their importance to the understanding of biological microfluidic systems, such as flow in blood vessels[113] and propulsion of microorganisms.[114] The compliance of a surface has the potential to significantly influence interaction with flows, with soft surfaces having been shown to significantly reduce drag in turbulent flows.[115]

Only two studies that we are aware of investigated the boundary conditions for flow of liquids over grafted polymer brushes.[116] This is a field that definitely deserves more attention, due to the great versatility and potential applicability of polymer brushes in microfluidics (for examples see Section 5.4.1) However, the presence of a soft layer chemically adsorbed onto the substrate makes the analysis of the slip data more difficult; for example, in hydrodynamic force measurements it complicates the obtainment of the calibration factor to convert cantilever deflection into forces, and to establish the zero of separation. In their study McLean *et al.* investigated the interaction and hydrodynamic forces between layers of the physisorbed triblock copolymer Pluronic in salt solutions by colloid probe AFM. [116] In this study the flow profile of the aqueous solution seemed to penetrate significantly into the polymer brush, but as the polymer was simply physisorbed on the surface, it is not clear how shear forces might have modified the interface during the experiment. Lanotte *et al.* studied the velocity profile of water in a microchannel coated with a grafted hydrophilic polymer brush and observed a slowdown of the flow with the swelling of the polymer brush compared to that of a bare channel.[117] They argued that the drag increase was due not only

to the decrease of the channel width after grafting, but also to the brush polydispersity and to flow perturbation generated by the shear of the grafted chains.

4.6 Slip Anisotropy

Anisotropy of the liquid flow is a subtle effect that is hard to appreciate in physical experiments. Preferred flow directions may arise either from the geometry of the technique used for the investigation or from the structures on the surface. In the case of drainage experiment (SFA, CP-AFM), where a sphere is made to approach a flat, the liquid flows in an isotropic manner over the surface away from the contact area as the two surfaces approach. In other techniques, such as optical techniques using flow tracers, the liquid flow, which is studied through a channel or between planar surfaces, is unidirectional. The structures fabricated on a surface may be isotropic (hexagonal arrays of pillars) or anisotropic in geometry (grooves, square arrays of pillars). Combining the flow directions with the orientations of the structures can lead to various cases with different slip properties. As a simple example, a channel structured with grooves can result in two different boundary conditions, depending on whether the flow is parallel or transverse to the alignment of the grooves. In physical experiments, an effective slip length, as defined in Section 2.5, is likely to be obtained, rather than an intrinsic slip length.[80, 86] The details of slip anisotropy are best investigated and understood through numerical simulations, as detailed in Section 5.2.

5 Computational Experiments on Interfacial Slip

The number of molecular and particle-based simulations of flow on complex surfaces has increased as the computational power required to run them has become more readily available. A major advantage of simulations compared to physical experiments for the study of flow over complex surfaces is that the variations in topography and boundary condition of the surface are entirely known. In the case of periodic structures, the period, amplitude, and average height values are important characteristics affecting the boundary condition. Because all aspects of the topography in a simulation are known, it is important to consider the authors' choice of reference surface when comparing simulations, as described in Section 2.3. In this section we will describe trends in the slip lengths measured with respect to the highest surface points, as depicted in Figure 2, such that it represents the difference between the physical and hydrodynamic boundaries of the surface. This is the slip length measured by many experimental techniques including AFM and SFA, and is the most relevant property in many practical scenarios.

Computational simulation methods commonly used in the study of flow over patterned surfaces include molecular dynamics, dissipative particle dynamics, and lattice Boltzmann simulations, all of which are particle-based methods. Another approach is to develop mathematical models by applying the Stokes equation to simple periodic geometries which may be solved analytically or numerically depending on the complexity of the problem.[42, 118-122] A major advantage of the particle-based techniques is that they can be applied to arbitrarily complex geometries, even including surfaces extracted from AFM topography images.[123]

Molecular dynamics simulates the movement of particles according to the classical equations of motion, with forces applied to each particle based on the interaction potentials defined for nearby particles.[124] These simulations are often "coarse-grained" such that individual molecules are modeled as spherical particles interacting via Lennard-Jones potentials, in order to increases the speed of the computation for a given system size and simulated time frame while maintaining liquid-like behavior. Modeling individual molecules allows the effect on the boundary condition of

roughness on the atomic scale to be studied, and shows variations in the liquid structure near the interface.[125-127]

Not all particle-based simulations model individual atoms or molecules. Dissipative particle dynamics[128] and lattice Boltzmann simulations[129] describe the motion of fictive particles each of which correspond to a fluid element representing a large number of molecules, which behave in such a way as to resemble a Newtonian liquid. These have been referred to as mesoscopic simulations, as they can access larger time and length scales than molecular dynamics simulations. Dissipative particle dynamics operates in a similar fashion to molecular dynamics except that viscous dissipative forces and random thermal forces are also applied to the particles. Lattice Boltzmann simulations solve the Boltzmann equation by discretizing particle positions onto a lattice. Compared to molecular dynamics, dissipative particle dynamics and Lattice Boltzmann simulations improve computational efficiency at a loss of atomic and molecular detail.

The slip length in molecular dynamics and dissipative particle dynamics has been shown to be determined by the strength of the attractive interaction between solid particles and liquid particles.[35, 36] A strong attraction, relative to thermal energies, results in a no-slip boundary condition, while a weaker attraction can result in slip by reducing the friction between substrate and liquid. In lattice Boltzmann simulations a repulsive interaction can be added to induce slip at the interface.[130]

5.1 Slip on Rough and Structured Surfaces

In this section we will discuss the effect of topographical roughness and structure on the boundary condition of fluid flow as studied by numerical simulations. Simulations have shed important light on issues with regard to the proper placement of the boundary surface,[66, 122, 123, 130] as discussed in Sections 2.3 and 4.1.3. They also help reveal some general trends on how the effective slip length depends on the geometric length scales of the roughness. In most simulation studies, surfaces with periodic topographical patterns are used as models to study rough surfaces, including those illustrated in

Figure 10, such as sinusoidal grooves (

Figure 10(a)), [40, 125, 127, 131] and square or triangular grooves (

Figure 10(b)).[66, 123, 130] Randomly generated statistical roughness has also been employed (

Figure 10(c)),[66, 123, 130, 132, 133] as well as surfaces generated from experimental AFM topography data.[66, 123, 132] In molecular dynamics, roughness on the molecular scale may be induced by varying the size of the atoms composing the solid relative to the fluid atoms (

Figure 10(d)).[126]

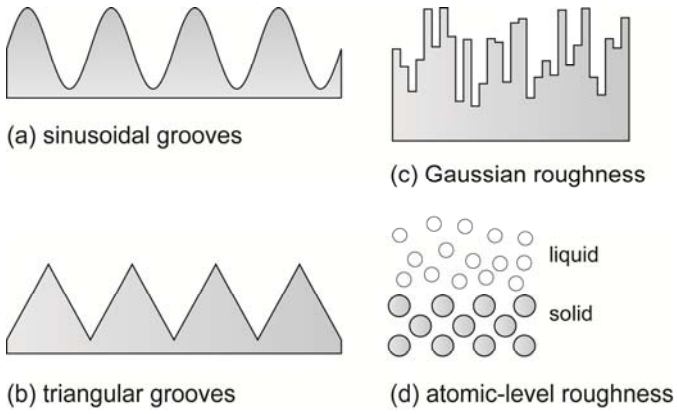

Figure 10: Some examples of models of rough/structured surfaces used to study effective boundary conditions in computational simulations, including (a) sinusoidal grooves, (b) triangular grooves, (c) Gaussian roughness, and (d) atomic level roughness, where the model solid atom size is increased relative to the liquid atom size. Part (d) adapted from [126] with permission.

5.1.1 Describing the Boundary Conditions

Analytical results derived by Panzer *et al.* for sinusoidal height variations demonstrate that the shifted boundary approach described in Section 4.1.3 is valid for large wavelengths in which higher order terms may be neglected.[122] The problem cannot be solved theoretically for shorter wavelengths or other geometries due to the difficulty in calculating higher order terms, however simulations have no such limitations.

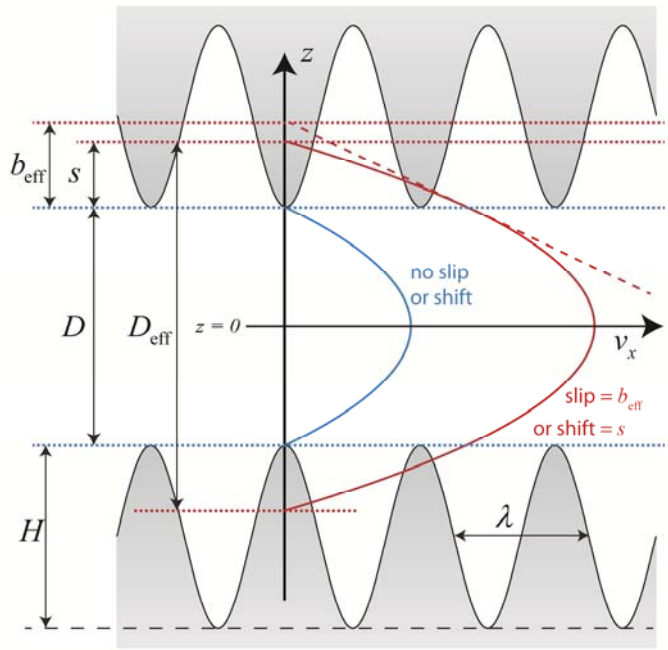

Figure 11: Schematic illustrating possible definitions of the boundary condition at a rough surface. A sinusoidal surface is illustrated, but the concept extends to other forms of roughness or structure. The blue solid line indicates a Poiseuille flow velocity profile for a no-slip boundary condition and the red one flow for which the velocity is non-zero at the top of the features. Two possible definitions of boundary condition of the latter are illustrated: a Navier slip boundary condition, characterized by an effective slip length, and a shifted boundary condition in which an effective no-slip wall is placed a distance *s* from the boundary. (To be reproduced in color)

In the case of Couette flow, there is no difference between the Navier and shifted boundary approaches because of the linearity of the velocity profile across the channel. In pressure-driven

Poiseuille flow the difference can be significant, as illustrated in Figure 11. The velocity profile for Poiseuille flow with a Navier slip boundary condition, with an effective slip length b_{eff}, obeys:[134]

$$v_x(z) = \frac{1}{2\eta}\frac{\partial P}{\partial x}\frac{D^2}{4}\left(1 - \left[\frac{2z}{D}\right]^2 + \frac{4b_{\text{eff}}}{D}\right) \qquad \textbf{(4)}$$

where v_x is defined in Figure 11, D is the channel width, η is the viscosity, and $\partial P/\partial z$ is the pressure gradient. For the case where a shifted effective no-slip boundary is assumed at a distance s from the top of the roughness, such that the effective channel width is $D_{\text{eff}} = D + 2s$, the velocity profile is:

$$v_x(z) = \frac{1}{2\eta}\frac{\partial P}{\partial x}\frac{D^2}{4}\left(1 - \left[\frac{2z}{D}\right]^2 + \frac{4s}{D} + \left[\frac{2s}{D}\right]^2\right) \qquad \textbf{(5)}$$

The difference due to the $(2s/D)^2$ term can be neglected for large values of D, but the difference can become dramatic for narrow channels, where it is comparable to or greater than that channel width. If the channel width is changed, either the slip length or shift value can remain constant, but not both. To our knowledge no systematic Poiseuille flow study has been conducted in which D is varied while holding all other parameters constant. Some support for the shifted surface model comes from lattice Boltzmann simulations performed by Kunert and Harting,[123] in which the channel width was decreased by increasing the amplitude of a Gaussian roughness; the fitted s increased linearly, while the fitted b_{eff} increased linearly for low roughness but much more rapidly for high roughness, for which s was a significant fraction of D.

A further complication is added when an intrinsic slip length (that of the equivalent flat interface) is non-zero. In this case the effective far field boundary will be the result of interplay between the influence of the roughness and the finite local slip. While it is not immediately clear how the boundary condition should be described in this case, one approach is to first determine the shifted surface position s on a surface with an intrinsic slip length of zero. Then, perform the same experiment on a surface with a finite intrinsic slip length, and fit an effective Navier slip length using this shifted boundary position as the reference surface.[132] In a simulation, with full control over the intrinsic slip length, both the boundary shift due to roughness and the slip length due to local slip can be determined independently, however in a physical experiment this would be far more challenging. To our knowledge, no underlying physical justification exists to support this approach, and there is great scope for further studies into correct description of the effective boundary condition in the presence of both finite intrinsic slip and surface roughness or structure. One possible approach could be to obtain both s and b_{eff} for a surface by subjecting the system to two different types of flow, such as Couette flow and Poiseuille flow. This approach, which provides enough information to fit both parameters, was used by Joly and collaborators for a complex superoleophobic system.[101, 135, 136]

5.1.2 Dependence of Boundary Conditions on Roughness Length Scales

A number of simulations reveal qualitative trends that appear to arise regardless of the details of the surface structure. These trends are illustrated in Figure 12. For a surface with a local no-slip boundary condition, as the amplitude of the roughness is increased from zero the effective slip increases.[123, 132] This is a fairly intuitive result: as regions of the surface are lowered below the

maximum height, liquid is able to flow within these depressions and thus the effective friction is decreased. The deeper the depressions (and the higher the roughness amplitude), the larger this effect.

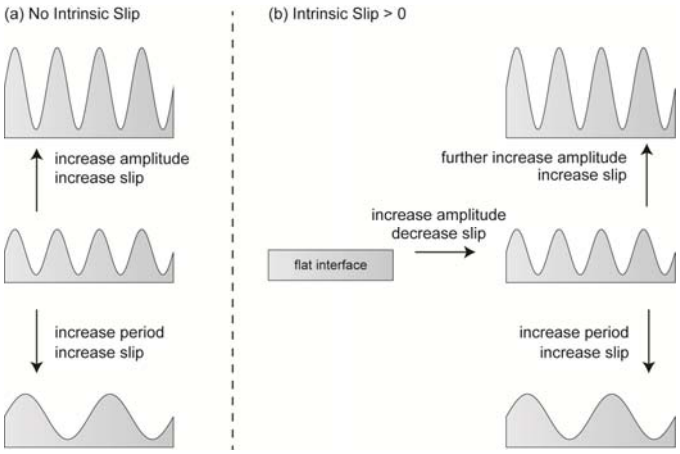

Figure 12: Summary of the effects of changes in roughness on the effective slip length at rough surfaces with (a) a local no-slip boundary condition at the true solid-liquid interface, and (b) a local slip boundary condition. Sinusoidal roughness is used as an example, but the trends appear to apply for other roughness geometries. Results adapted from references [123, 125-127, 132].

The behavior changes if the local slip length at the solid-liquid interface is non-zero (Figure 12(b)). Numerous studies suggest that if the amplitude is comparable or smaller than the slip length, then as the amplitude is increased the effective slip is reduced. This can be understood as the corrugations in the surface causing additional friction between the fluid and the solid.[125, 127, 132] However as the amplitude is increased to very large values relative to the local slip length, the effective slip increases, as for the case when no local slip is present.[126, 132] Lattice Boltzmann simulations by Kunert *et al.* suggest that when the amplitude is large compared to the local slip, the slip may be significantly enhanced compared to the location of the shifted boundary, because of a reduced pressure near the hydrophobic interface presenting a smoothed effective surface to the fluid.[132] However, few simulations have probed this regime, and we believe there is ample scope for further studies of the effect of roughness amplitude on the effective boundary condition in the presence of local slip, particularly as the amplitude becomes large compared to the local slip length.

The other relevant length scale is the period of the roughness. In this case the effect is similar regardless of the intrinsic slip at the interface. A decrease in the period of the roughness decreases the effective slip.[123, 125, 127] For a short enough period even an intrinsically high slip surface, or one with large roughness amplitude, can be rendered effectively no-slip. This effect is particularly dramatic when modeling atomic level roughness using molecular dynamics simulations. For example, in molecular dynamics simulations by Priezjev *et al.*, a no-slip effective boundary condition was found at a surface with an intrinsic slip length (that of the smooth surface) of 10 molecular diameters, a period of a 1.82 molecular diameters, and amplitude of only 0.086 molecular diameters.[127] Displacement of the wall atoms in this case was a factor of 100 smaller than the slip length of the smooth surface.

The dramatic slip-suppressing effect of atomic level roughness demonstrated by simulations raises the question of why finite slip lengths, on the scale of tens of nanometers, have been measured experimentally on surfaces such as hydrophobized silicon wafers which have a finite roughness on the nanometric scale.

5.2 Slip on Chemically Heterogeneous Surfaces

In addition to variations in topography over a surface, the boundary condition for liquid flow may be affected by local variations in surface chemistry across a surface on nano- or microscopic scales. Different local surface chemistries may of course lead to different local slip lengths. In the extreme case of a nanobubble-laden surface,[121, 137, 138] or a rough hydrophobic surface with trapped air cavities,[101, 139-141] regions of the surface may have perfect slip boundary conditions at a liquid-air interface, greatly reducing the effective friction between liquid and boundary.

Continuum and molecular dynamics simulations have shown that a chemically heterogeneous surface induces complex flow patterns near the interface.[42] As the liquid flows, it encounters regions with different slip length, and it will increase or decrease its velocity in the flow direction to compensate. In order to conserve momentum this results in non-zero velocity components perpendicular to the direction of shear.[118, 142, 143] Analysis of the streamlines in molecular dynamic simulations by Karakare *et al.* shows that a patterned boundary condition can induce rotational flow structures similar to those normally seen only in turbulent flow at much higher Reynolds number,[39] in a similar manner to the complex flow induced by roughness, as discussed in Section 5.1. This turbulent behavior can be exploited in order to significantly enhance the mixing of liquids on the nano-scale.[42, 144-147] The optimal conditions for mixing are when the pattern length matches the width of the channel, which maximizes the transverse flow velocity.[42]

In Section 5.2.1 we will discuss some useful general principles in predicting the effective slip length at chemically heterogeneous surfaces.[43, 119, 120, 140, 141, 143, 148] We will then look at the effect of introducing roughness as well as patterning in the case of protruding gas regions in Section 5.2.2. [87, 118, 121, 137, 138] Finally, we will cover the angular dependence of the effective slip over anisotropic surfaces in Section 5.3.[118, 119, 142, 143, 149]

5.2.1 The Effective Slip Length at Chemically Patterned Surfaces

While the flow near a chemically-patterned interface is complex, further from the substrate the variations average out and the flow velocity becomes more homogeneous. This is the case for flow at a distance from the interface significantly greater than the length scale of the local variations in slip length. It has been proposed that, in this far-field region, the flow velocity profile is equivalent to that which would result from a chemically homogeneous surface with a slip length b_{eff} . The case of b_{eff} for an arbitrary pattern of slip length $b(x, y)$ is too complex a problem for a general expression to be derived, but in certain limiting cases approximate expressions have been proposed. These will be briefly summarized in this section.

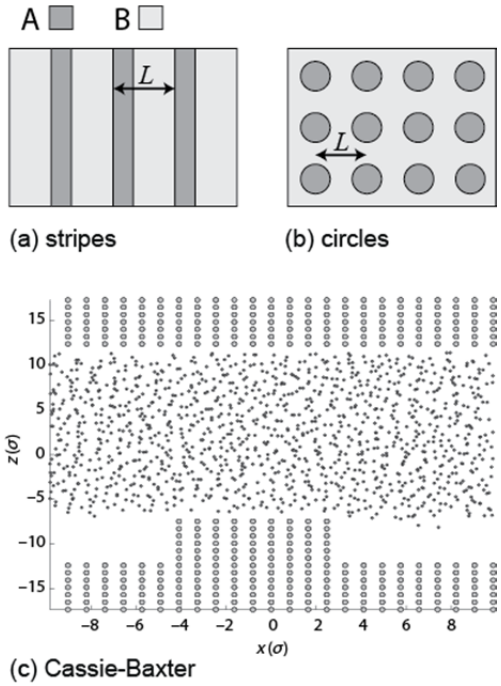

Figure 13: Illustration of common types of model surfaces used to study binary chemically patterned surfaces, including simple geometries: (a) stripes, (b) circles; and (c) more complex model interfaces in the Cassie-Baxter regime.[139] Part (c) adapted from [139] with permission.

Depicted in Figure 13 are the most commonly studied model systems in simulations, which are surfaces with two types of surface chemistry, which we will refer to as "A" and "B" with different local slip lengths b_A and b_B respectively, each of which covers a fraction of the surface ϕ_A and $1-\phi_A$. These regions are arranged into a pattern with some characteristic length scale L, which might be regular stripes, circles, or some randomly generated arrangement. The effective slip length in this case depends not only on the slip lengths of the two components and the fraction of the surface they cover, but also on the length scale of the variations in local slip relative to the slip lengths themselves. In Figure 13(a) and (b) the differences in intrinsic slip length between the two components would be created by varying the strength of the liquid-solid interaction potential, while in (c) a Cassie-Baxter state is induced resulting in a pattern of liquid-vapor and liquid-solid interfaces with different intrinsic slip lengths.[139]

Hendy and Lund [43, 120] used a perturbative analytical approach to derive approximate expressions for the effective slip length. The appropriate relation depends on the relative length scales of the system, b_A, b_B, and the pattern length scale L. In the case where b_A and $b_B \ll L$, the effective slip length is approximated well by taking an arithmetic mean weighted by the area:

$$b_{eff} = \phi_A b_A + (1-\phi_A) b_B \qquad (6)$$

However in the case b_A and $b_B \gg L$, the effective slip length is approximated by:

$$\frac{1}{b_{eff}} = \frac{\phi_A}{b_A} + \frac{(1-\phi_A)}{b_B} \qquad (7)$$

This expression is similar to that used to calculate electrical resistance for resistors connected in parallel. This relation was initially proposed by Cottin-Bizonne *et al.* as a phenomenological

model.[140] It is in effect taking a weighted average of the friction coefficients η/b to get an effective friction coefficient, inversely proportional to the effective slip length. There is an exception to Eq. 7 when b_A and b_B are much larger than L , but are comparable to each other. In this case, Eq. 6 provides the better estimate of the effective slip length. In addition, recent work by Asmolov *et al.*[150] has shown that Eq. 6 may overestimate the slip length at weakly slipping patterned surfaces if there are sharp step-like transitions between the two components A and B, which can create additional friction.

A particular case that has attracted significant interest is that in which one component of the surface has either very high or perfect slip, while the other has little or no slip relative to the pattern length scale. Such a surface is an analogue for both superhydrophobic surfaces and those covered with nanobubbles. In the case of $b_A = \infty$ and $b_B = 0$, no general approximation for the effective slip length has been proposed, but a number of geometry specific expressions have been derived.[119, 134, 140, 141]

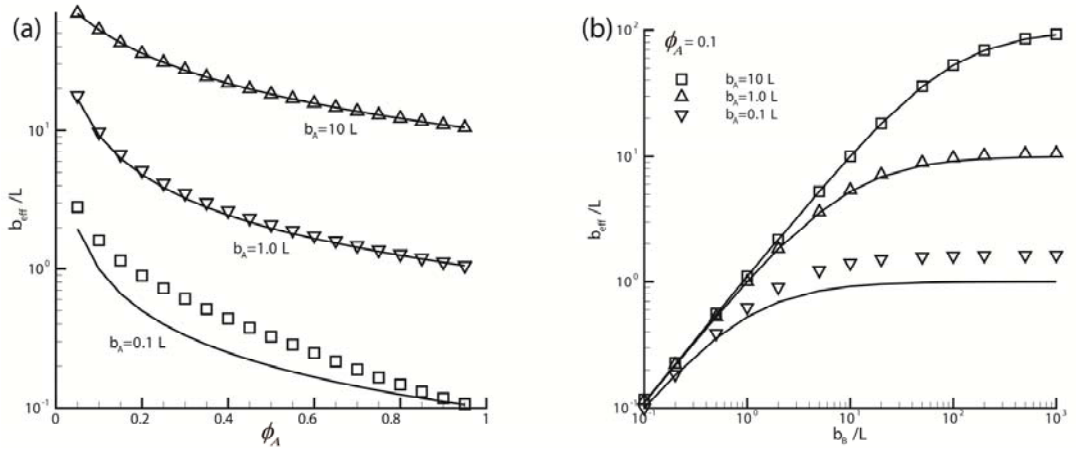

Figure 14: Effective slip length b_{eff} over stripes with period L calculated by finite difference solutions of the Laplace equation (symbols) and Eq. 7 (solid lines) as (a) a function of coverage fraction ϕ_A (the fraction of the surface with intrinsic slip length b_A) for intrinsic slip lengths $b_A = 0.1 - 10L$ and $b_B = 100L$, and (b) as a function of b_B for $b_A = 0.1 - 10L$ and $\phi_A = 0.1$. Figures adapted from [120] with permission. Notation has been modified to match that used in this article.

Simulations have been used both to investigate these limiting cases and test the validity of the approximations, as well as to probe intermediate cases for which simple analytical expressions elude us. Continuum hydrodynamics simulations allow the flow equations to be solved numerically with fewer approximations and are consistent with the results. Cottin-Bizonne *et al.* [140] showed that continuum simulations for flow over perpendicular stripes alternating between partial and infinite slip agree with Eq. 7, and also suggest the lower slip length can be a factor of 10 lower than the pattern period before the model fails. Similar simulations by Hendy and Lund [120] confirm that Eq. 7 applies in the appropriate limit, as shown in Figure 14, and that it breaks down when the slip lengths are small compared to pattern length.

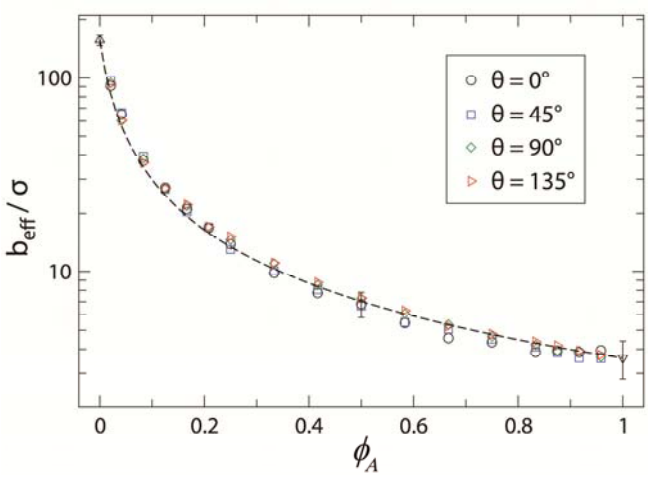

Figure 15: Effective slip length as a function of coverage fraction ϕ_A (the fraction of the surface with intrinsic slip length b_B) as measured by molecular dynamics simulations of flow over surfaces with randomly distributed slip and no-slip solid atoms for $b_A = 3.6\sigma$ and $b_B = 156\sigma$ where the Lennard-Jones parameter σ is approximately one molecular diameter. The inset specifies the orientation of the direction of shear. The dashed line represents Eq. 7. Figure adapted from [143] with permission.

Eq. 7 also appears to describe highly random patterns well. In molecular dynamics simulations by Priezjev[143] two types of solid atoms, one with a strong and one with a weak attraction to fluid particles, corresponding to low and high slip respectively, were randomly distributed across a surface, presumably leading to a characteristic length on the order of the molecular size (σ) such that $b_A >> L >> b_B$. As shown Figure 15, the effective slip length was very well described by the theory suggesting it could be an effective model for surfaces with random heterogeneity on the atomic scale. This suggests that Eq. 7 may offer a guide to creating surfaces with a tunable slip length by mixing functional groups with known intrinsic slip lengths.

5.2.2 Protruding Bubbles

In the interesting case of the effective slip over nanobubble and Cassie-state superhydrophobic interfaces on which one of the pattern components is air, there is an additional complication due to the curvature of the liquid-air interface. Several studies have investigated the impact of this protrusion on the effective slip length of the interface. Simulations allow the protrusion angle, as shown in Figure 16 to be finely tuned.

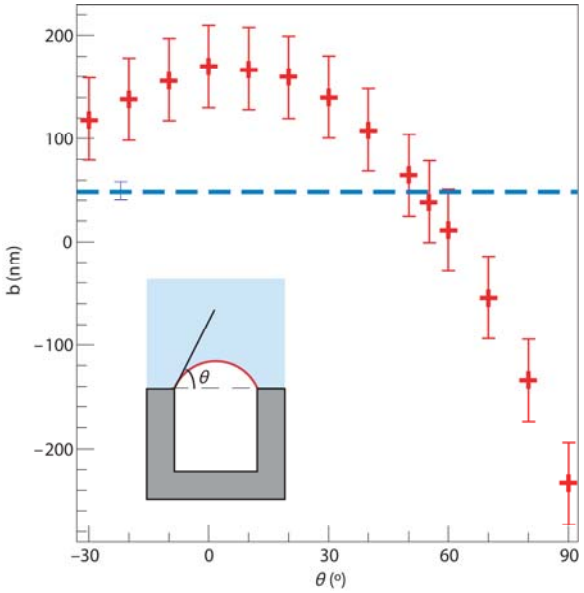

Figure 16 Evolution of the slip length (+) with the meniscus shape on a Cassie interface. The interfacial slip length on a wetted Wenzel interface was obtained numerically and is represented with the dashed line. A schematic representation of the meniscus is depicted in the inset. Adapted from Steinberger *et al.* [87] with permission.

As might be expected, as the protrusion angle is increased from zero degrees, the effective slip length as measured with respect to the flat solid surface is reduced. For small angles, the high local slip length at the air-liquid interface causes the effective slip length to be higher that of the slip at the solid-liquid interface, but for a high enough protrusion angle the roughness inhibits the slip to the point that higher flow velocities would be achieved if the air regions were not present at all.[87, 118, 121, 138] In the case of nanobubbles it has been suggested that based on experimentally known properties, the increase in the effective slip length due to their presence may actually be negligible due to this effect.[137]

5.3 Angular Dependence of the Effective Slip Length

If the pattern of slip or topographical structure on the surface is anisotropic, for example a surface with parallel stripes of different slip length, then it has been found that the effective slip length depends on the orientation of the pattern relative to the direction of shear. A number of studies have compared flows parallel and perpendicular to the direction of a striped pattern, and at arbitrary angles. In general, the effective slip length is at a maximum when the flow is parallel to the stripes, and at a minimum when perpendicular.[118, 119, 134, 142, 149-152]

For a given angle $0° < \theta < 90°$ the solution to the Stokes equations when the stripe width is much smaller than the channel width gives an effective slip length according to:

$$b_{\text{eff}}(\theta) = b_{\perp}\cos^2\theta + b_{\parallel}\sin^2\theta \qquad \textbf{(8)}$$

Where $b_{\perp}$ and $b_{\parallel}$ are the effective slip lengths perpendicular and parallel to the direction of shear.[151, 153, 154] Molecular dynamics result have been consistent with this expression,[143] with best agreement for larger stripes, and a slight discrepancy as the stripe width approached the molecular scale.

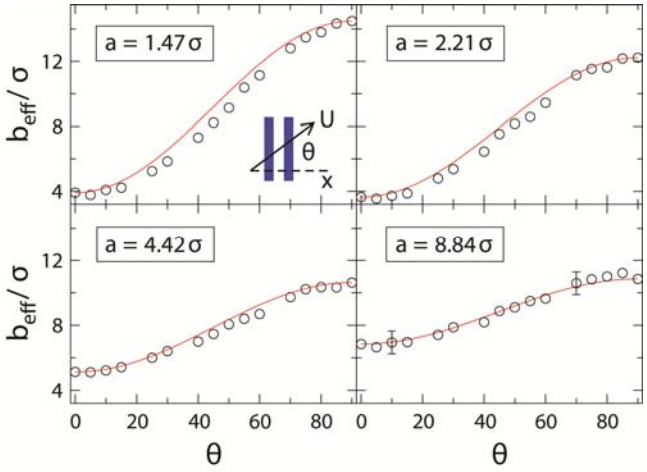

Figure 17: Comparison between continuum hydrodynamic prediction (solid lines) and molecular dynamics simulation results for effective slip length as a function of shear angle for flow over stripes of equal width *a* with different wettabilities. Adapted from [143] with permission.

In the case of perpendicular stripes or grooves there will be a non-zero component of the velocity normal to the surface. When the flow is at an angle neither parallel nor perpendicular to the pattern, the flow will also have a non-zero velocity in the plane of the surface and perpendicular to the direction of shear. This can be exploited to further enhance the mixing effects described in the previous section. In the case of parallel stripes, the ratio of the perpendicular to parallel velocity components is given by:[153]

$$\frac{v_\perp}{v_\parallel} = \frac{(b_\parallel - b_\perp)\sin\theta\cos\theta}{b_\perp \cos^2\theta + b_\parallel \sin^2\theta} \qquad \textbf{(9)}$$

This was in qualitative agreement with molecular dynamics simulations by Priezjev et al [143] but the theory consistently overestimated the simulation result, as shown in Figure 17, which the authors speculated may have been the result of the atomic scale roughness in the surface. Jeon *et al.* [142] showed that the flow velocity through cylindrical nanochannels patterned with helical stripes increases monotonically as the stripe angle is increased from zero degrees (perpendicular) to 90 degrees (parallel).

5.4 Slip on Polymer Brushes

A polymer brush is a particular type of rough surface, as there are many situations in which significant flow might occur within the brush. For this reason there are alternative ways to define slip in the case of the brush. The boundary condition at a polymer brush can be characterized by two parameters: i) an effective penetration length, l_p as shown in Figure 18 – the distance from the top of the brush to the point at which the flow extrapolates to zero, analogous to a slip length; ii) the stagnation length, l_s also illustrated in Figure 18 – the distance from the solid substrate at which flow occurs, analogous to a negative slip length.

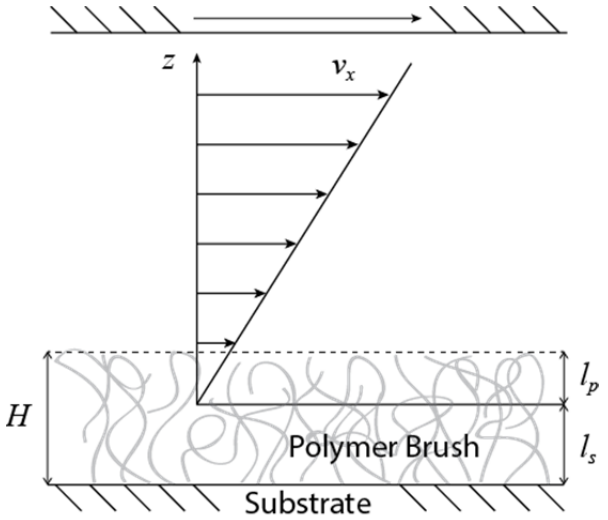

Figure 18: Couette flow over a polymer brush induced by moving a top bounding wall at a constant velocity to generate a linear flow velocity profile. The stagnation length, l_s, is the distance from the substrate at which the flow appears to be completely inhibited by the brush. The penetration length, l_p, is the difference between the stagnation length and the brush height and is analogous to the slip length. Figure adapted from [155] with permission.

There have been a number of simulation studies on polymer brushes in a flowing Newtonian liquid, [38, 114, 156-174], although not all of these are concerned with characterization of the boundary condition. The flow of liquids within polymer brushes (and polymer solutions in general) has been modeled in terms of the Brinkman equation,[169, 175] originally developed to describe flow within porous materials. In the case of polymer brushes, the pore size is substituted by the correlation length of the polymer ξ, which is a function of the polymer volume fraction ϕ. For the flow of a liquid with velocity v in the x direction within a polymer brush, the Brinkman equation becomes:[169]

$$\frac{\partial^2 v}{\partial x^2} = \frac{v}{\xi^2(\phi)} \qquad \textbf{(10)}$$

In the following Section we will describe computational studies of flow over polymer brushes, and their potential application as functional surfaces for controlling fluid flow.

Many of the computational studies into the effect of liquid flow on polymer brushes proceed using an implicit solvent approach, where solvent particles are not modeled but are simulated by applying random forces to the polymers to simulate collisions with solvent particles.[164, 165, 167, 176] Additional forces are then applied to the polymer based on the assumption that the flow will be in accordance with the Brinkman equation, allowing the effects of the flow on polymer conformation to be modeled. Employing an implicit solvent, rather than explicitly including solvent particles in the simulation, greatly reduces the computational expense, but does not allow the boundary condition to be tested and prevents the observations of details of the polymer dynamics.

We have conducted molecular dynamics simulations of short-chain polymer brushes under the Couette flow of an explicit solvent, as depicted in Figure 18.[155] We found that the penetration length of the flow, defined above, increased linearly with the distance between chain anchor points, or the inverse square-root of the grafting density. This is in qualitative agreement with the Brinkman equation, given that the correlation length within a polymer brush scales in proportion with the distance between chain anchor points. The stagnation length – or the effective hydrodynamic thickness of the brush – appeared to scale with the grafting density as $\rho^{1/3}$. This is the same scaling

law expected for the height in the limit of long chain brushes. Wijmans *et al.*[177] also found that the penetration length of the flow increased with decreasing grafting density.

Several molecular dynamics studies have observed an interesting detail in the polymer dynamics: the direction of the flow is reversed a short distance into the polymer brushes, with the chains undergoing a tumbling motion.[155, 163, 166, 170] The impact of this behavior on the flow in the far field is likely to be subtle, but the effect illustrates the necessity of explicit-solvent molecular dynamics studies in their ability to resolve such behavior.

5.4.1 Switchable Surfaces: Valves and Mixers

By changing the quality of the solvent, polymer brushes can be swollen and collapsed reversibly. It has been suggested that the significant reduction in height on collapse could be exploited for use in valve in nanosized capillaries.[156, 160, 171, 173, 178] When swollen, the polymer chains could extend across a sufficiently narrow capillary and significantly inhibit the flow of liquid. When collapsed the effective diameter of the capillary increases allowing liquid to flow. A variety of triggers might be used to initiate the switch including temperature, pH, ionic strength,[179] or electric fields,[171] depending on the chemistry of the polymer.

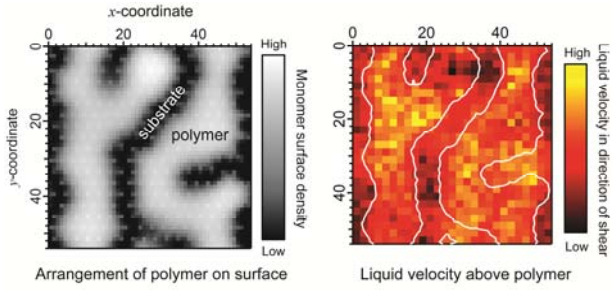

Figure 19: Molecular dynamics simulations of flow over dewetted polymer brushes. Part (a) shows the density distribution of a collapsed polymer having undergone constrained dewetting. Part (b) shows the flow velocity in the direction of shear (left to right) immediately above the collapsed polymer layer. A slip boundary condition applies at the liquid-polymer interface, while a no-slip condition applies at the liquid substrate interface. The velocity of the fluid immediately about the polymer is significantly greater than that above the no-slip substrate. Adapted from reference [155] with permission. (To be reproduced in color)

Below a critical grafting density, collapsed polymers self-assemble into patterns on the surface through a process known as constrained dewetting.[180, 181] Figure 19 illustrates our recent molecular dynamics simulations demonstrating that such a surface could be used to create a surface with patterned slip length and complex flow near the interface, similar to those described in Section 5.2.[155] In such a system the pattern could be turned on and off by switching between the swollen and collapsed state, which could allow the polymer brush to be employed as a switchable nanofluidic mixer.

6 Conclusions and Outlook

From this overview of the recent literature on interfacial slip we can observe that the field is rapidly reaching maturity and expanding to new areas. Numerous investigations have addressed the question of how surface characteristics such as texturing, tailored roughness, stiffness, and presence of adsorbed gas affect the occurrence and magnitude of liquid slip. In particular, new trends are emerging that aim to exploit novel surfaces which mimic engineered properties present in nature, such as the drag-reducing properties of the lotus leaf. However we believe there are aspects that still deserve more attention, such as:

- *Slip over soft surfaces* Most biological liquids, such as blood in capillaries, flow in confined geometries, and it is tempting to think that nature would have perfected the surface design to facilitate flow. In the engineering field, it is fairly well established that soft surfaces are capable of reducing the growth of disturbances in a laminar boundary layer and thus possess the potential for reducing drag at the interface with a solid. For example, the skin of several aquatic animals is textured with cilia, which have the effect of reducing interfacial drag while swimming.[182] In all of these real-world situations flow occurs over soft and compliant surfaces. Physical experiments designed to test interfacial slip on soft surfaces are rare, due to the complication and uncertainty introduced by the presence of a soft interface. Natural candidates to prepare soft surfaces are grafted polymer layers, which offer versatile and tunable properties. It would be very interesting to be able to expand research in this direction, to improve both our fundamental understanding of interfacial slip of biological and real-world systems, and to improve our design of microfluidic and nanofluidic devices.
- *More stable slippery surfaces* The design of complex superhydrophobic surfaces that can delay the Cassie-to-Wenzel transition to smaller solid fractions is a challenge that needs addressing, in order to increase the effective slip length on more stable surfaces. Hierarchical surfaces appear to be the most effective in terms of large slip values. A possible approach might include developing superhydrophobic hierarchical surfaces where the main microstructures are separated by smaller microstructures that could offer more support to resist the liquid pressure.
- *Rough surfaces with intrinsic slip* There remains a gap in our understanding of the boundary condition in the case of interfaces with both roughness or structure and a non-zero intrinsic slip length. Part of the confusion comes from uncertainty in the position in the reference surface from which the slip length is measured in such a case. Some insights have been obtained in simulations by comparing Poiseuille flow over a particular geometry with intrinsic slip with flow over the same geometry with no slip, using the latter to locate a reference surface and the former to fit the slip length.[132] A better approach may be to compare the same geometry under different flow types, allowing the position of the reference surface to be fitted simultaneously with the effective slip length.[183] This is a simple procedure in nanochannel experiments, in which similar code can probe both Couette and Poiseuille flow, albeit with a doubling of the compute time. In physical experiments conducting equivalent experiments with different flow types is more challenging, but might be achieved for example by comparing liquid drainage experiments performed by SFA with lateral shearing experiments also by SFA.
- *Discrepancies between computational and physical studies* Computational studies suggest that short-period variations in topography can reduce the effective slip to near zero even when the peak-to-valley variation is small compared to the slip length. This observation would appear to be in conflict with the results of AFM-CP experiments in which a significant slip is measured on surfaces such as hydrophobized silicon wafers, for which the atomic level roughness might be expected to inhibit any slip. For relatively smooth surfaces, it has been found that, while slip is observed in molecular dynamics simulations, the slip length is far smaller than that measured by experiments. The comparison is complicated by the mismatch in the shear rate, which in molecular dynamics is much greater than that accessible experimentally, possibly contributing to the mismatch in reported slip lengths. Further studies bridging the shear rate gap between experiments and simulations are required.

7 Acknowledgements

The authors wish to thank the Australian Research Council for funding.

8 References

[1] Bocquet L, Charlaix E. Chem Soc Rev. 2010;39:1073-95.
[2] Goldstein S. Annu Rev Fluid Mech. 1969;1:1-28.
[3] Neto C, Evans DR, Bonaccurso E, Butt H-J, Craig VSJ. Rep Prog Phys. 2005;68:2859-97.
[4] Vinogradova OI. Int J Miner Process. 1999;56:31-60.
[5] Pit R, Hervet H, Léger L. Phys Rev Lett. 2000;85:980-3.
[6] Craig VSJ, Neto C, Williams DRM. Phys Rev Lett. 2001;87:054504.
[7] Bonaccurso E, Kappl M, Butt H-J. Phys Rev Lett. 2002;88:76103.
[8] Dong HY, Cheng MJ, Zhang YJ, Wei H, Shi F. J Mater Chem A. 2013;1:5886-91.
[9] Park KC, Choi HJ, Chang CH, Cohen RE, McKinley GH, Barbastathis G. ACS Nano. 2012;6:3789-99.
[10] Navier CLMH. Mem Acad Sci Inst Fr. 1823;6:389-416, 32-36.
[11] Vinogradova OI. J Colloid Interface Sci. 1995;169:306-12.
[12] Vinogradova OI. Langmuir. 1995;11:2213-20.
[13] Vinogradova OI. Langmuir. 1996;12:5963-8.
[14] Vinogradova OI. Langmuir. 1998;14:2827-37.
[15] Vinogradova OI, Butt H-J, Yakubov GE, Feuillebois F. Rev Sci Instrum. 2001;72:2330-9.
[16] Lauga E, Brenner MP, Stone HA. Microfluidics: the no-slip boundary condition. In: Foss J, Tropea C, Yarin A, (editors). Handbook of Experimental Fluid Dynamics. New-York: Springer; 2007. Chapter Chapter 19.
[17] Bonaccurso E, Kappl M, Butt H-J. Curr Opin Colloid Interface Sci. 2008;13:107-19.
[18] Bouzigues CI, Tabeling P, Bocquet L. Phys Rev Lett. 2008;101:114503.
[19] Tretheway DC, Meinhart CD. Phys Fluids. 2004;16:1509-15.
[20] Tsai PC, Peters AM, Pirat C, Wessling M, Lammertink RGH, Lohse D. Phys Fluids. 2009;21.
[21] Schaeffel D, Yordanov S, Schmelzeisen M, Yamamoto T, Kappl M, Schmitz R, et al. Phys Rev E. 2013;87:051001.
[22] Schmitz R, Yordanov S, Butt HJ, Koynov K, Dünweg B. Phys Rev E. 2011;84:066306.
[23] Yordanov S, Best A, Butt H-J, Koynov K. Opt Express. 2009;17:21149-58.
[24] Bolognesi G, Cottin-Bizonne C, Guene EM, Teisseire J, Pirat C. Soft Matter. 2013;9:2239-44.
[25] Chan DYC, Horn RG. J Chem Phys. 1985;83:5311-24.
[26] Zhu Y, Granick S. Phys Rev Lett. 2002;88:106102.
[27] Choi CH, Kim CJ. Phys Rev Lett. 2006;96.
[28] Ou J, Jonathan PR. Phys Fluids. 2005;17:103606.
[29] Zhu L, Attard P, Neto C. Langmuir. 2011;27:6712–9.
[30] Zhu L, Attard P, Neto C. Langmuir. 2011;27:6701–11.
[31] Zhu L, Attard P, Neto C. Langmuir. 2012;28:3465-73.
[32] Zhu L, Neto C, Attard P. Langmuir. 2012;28:7768–74.
[33] Barnes HA, Hutton JF, Walters K. An introduction to rheology. Amsterdam: Elsevier; 1989.
[34] Cottin-Bizonne C, Cross B, Steinberger A, Charlaix E. Phys Rev Lett. 2005;94:056102.
[35] Barrat J-L, Bocquet L. Phys Rev Lett. 1999;82:4671-4.
[36] Jabbarzadeh A, Atkinson JD, Tanner RI. J Chem Phys. 1999;110:2612-20.
[37] Pahlavan AA, Freund JB. Phys Rev E. 2011;83:021602.
[38] Pastorino C, Kreer T, Muller M, Binder K. Phys Rev E. 2007;76:026706.
[39] Karakare S, Kar A, Kumar A, Chakraborty S. Phys Rev E. 2010;81:016324.
[40] Niavarani A, Priezjev NV. Phys Fluids. 2009;21:052105-10.
[41] Al-Zoubi A, Brenner G. Comput Math Appl. 2008;55:1365-76.
[42] Hendy SC, Jasperse M, Burnell J. Phys Rev E. 2005;72:016303.
[43] Lund NJ, Hendy SC. ANZIAM J. 2009;50:381-94.
[44] Gadelmawla ES, Koura MM, Maksoud TMA, Elewa IM, Soliman HH. J Mater Process Tech. 2002;123:133-45.
[45] Israelachvili JN. J Colloid Interface Sci. 1973;44:259–71.
[46] Gupta R, Frechette J. Langmuir. 2012;28:14703-12.
[47] Israelachvili JN. Intermolecular and Surface Forces. 2nd ed. London: Academic Press; 1991.
[48] Bureau L. Phys Rev Lett. 2007;99:225503.
[49] Charrault E, Banquy X, Kristiansen K, Israelachvili J, Giasson S. Tribol Lett. 2013;50:421-30.
[50] Sun G, Bonaccurso E, Franz V, Butt H-J. J Chem Phys. 2002;117:10311-4.
[51] Granick S, Zhu Y, Lee H. Nature Mater. 2003;2:221-7.
[52] Bonaccurso E, Butt H-J, Craig VS. Phys Rev Lett. 2003;90:144501.
[53] de Gennes P-G, Brochard-Wyart F, Quéré D. Capillarity and Wetting phenomena. Drops, bubbles, pearls, waves. New York: Springer; 2004.
[54] Wenzel RN. Ind Eng Chem. 1936;28:988-94.
[55] Cassie ABD, Baxter S. Trans Faraday Soc. 1944;40:546-51.
[56] Lafuma A, Quéré D. Nature Mater. 2003;2:457-60.
[57] Schmatko T, Hervet H, Leger L. Langmuir. 2006;22:6843-50.

[58] Ligrani P, Blanchard D, Gale B. Phys Fluids. 2010;22.
[59] Hao PF, Yao ZH, He F, Zhu KQ. J Micromech Microeng. 2006;16:1397-402.
[60] Hetsroni G, Mosyak A, Pogrebnyak E, Yarin LP. Int J Heat Mass Tran. 2005;48:1982-98.
[61] Kandlikar SG, Joshi S, Tian SR. Heat Transfer Eng. 2003;24:4-16.
[62] McHale G, Newton MI. J Appl Phys. 2004;95:373-80.
[63] Du B, Goubaidoulline I, Johannsmann D. Langmuir. 2004;20:10617-24.
[64] Vinogradova OI, Yakubov GE. Phys Rev E. 2006;73:045302.
[65] Henry CL, Craig VSJ. Phys Chem Chem Phys. 2009;11:9514-21.
[66] Kunert C, Harting J, Vinogradova OI. Phys Rev Lett. 2010;105:016001.
[67] Rodrigues TS, Butt HJ, Bonaccurso E. Colloids Surfaces A. 2010;354:72-80.
[68] Guriyanova S, Semin B, Rodrigues TS, Butt HJ, Bonaccurso E. Microfluid Nanofluid. 2010;8:653-63.
[69] Barthlott W, Neinhuis C. Planta. 1997;202:1-8.
[70] Oner D, McCarthy TJ. Langmuir. 2000;16:7777-82.
[71] Byun M, Hong SW, Qiu F, Zou Q, Lin Z. Macromolecules. 2008;41:9312-7.
[72] Choi S-H, Zhang Newby B. J Chem Phys. 2006;124:54702.
[73] Joseph P, Cottin-Bizonne C, Benoit J-M, Ybert C, Journet C, Tabeling P, et al. Phys Rev Lett. 2006;97:156104.
[74] Lee C, Choi CH, Kim CJ. Phys Rev Lett. 2008;101.
[75] Lee C, Kim CJ. Langmuir. 2011;27:4243-8.
[76] Lee C, Kim C-JCJ. Langmuir. 2009;25:12812-8.
[77] Ou J, Perot B, Rothstein JP. Phys Fluids. 2004;16:4635-43.
[78] Truesdell R, Mammoli A, Vorobieff P, van Swol F, Brinker CJ. Phys Rev Lett. 2006;97:044504.
[79] Watanabe K, Takayama T, Ogata S, Isozaki S. AIChE J. 2003;49:1956-63.
[80] Bhushan B. Langmuir. 2012;28:1698-714.
[81] Bixler GD, Bhushan B. Soft Matter. 2013;9:1620-35.
[82] Maali A, Pan Y, Bhushan B, Charlaix E. Phys Rev E. 2012;85:066310.
[83] Yamada T, Hong C, Gregory OJ, Faghri M. Microfluid Nanofluid. 2011;11:45-55.
[84] Mongruel A, Chastel T, Asmolov ES, Vinogradova OI. Phys Rev E. 2013;87:011002.
[85] Karatay E, Haase AS, Visser CW, Sun C, Lohse D, Tsai PA, et al. Proc Natl Acad Sci USA. 2013;110:8422-6.
[86] Kashaninejad N, Nguyen NT, Chan WK. Phys Fluids. 2012;24.
[87] Steinberger A, Cottin-Bizonne C, Kleimann P, Charlaix E. Nature Mater. 2007;6:665-8.
[88] Dean B, Bhushan B. Phil Trans R Soc A. 2010;368:4775-806.
[89] Dean B, Bhushan B. Appl Surf Sci. 2012;258:3936-47.
[90] Voronov RS, Papavassiliou DV, Lee LL. Ind Eng Chem Res. 2008;47:2455-77.
[91] Rothstein JP. Slip on Superhydrophobic Surfaces. Annu Rev Fluid Mech. Vol. 422010. p. 89-109.
[92] Vinogradova OI, Dubov AL. Mendeleev Commun. 2012;22:229-36.
[93] Lee DJ, Cho KY, Jang S, Song YS, Youn JR. Langmuir. 2012;28:10488-94.
[94] Jung YC, Bhushan B. J Phys: Condens Matter. 2010:035104.
[95] Papageorgiou DP, Tsougeni K, Tserepi A, Gogolides E. Microfluid Nanofluid. 2013;14:247-55.
[96] Maali A, Bhushan B. Phil Trans R SocA. 2012;370:2304-20.
[97] Joseph P, Cottin-Bizonne C, Benoit JM, Ybert C, Journet C, Tabeling P, et al. Phys Rev Lett. 2006;97.
[98] Watanabe K, Yanuar, Udagawa H. J Fluid Mech. 1999;381:225-38.
[99] Philip JR. ZAMP. 1972;23:353-72.
[100] Byun D, Kim J, Ko HS, Park HC. Phys Fluids. 2008;20.
[101] Joly L, Biben T. Soft Matter. 2009;5:2549-57.
[102] Bhushan B, Wang Y, Maali A. Langmuir. 2009;25:8117-21.
[103] Busse A, Sandham ND, McHale G, Newton MI. J Fluid Mech. 2013;727:488-508.
[104] Zhang ZH, Zhang ZD, Lou ST, Zhang ZX, Sun JL, Hu J. Langmuir. 2004;20:3813-5.
[105] Zhang X-H, Li G, Maeda N, Hu J. Langmuir. 2006;22:9238-43.
[106] Zhang XH, Maeda N, Craig VSJ. Langmuir. 2006;22:5025-35.
[107] Lou ST, Gao J, Xiao X-D, Li X, Li G, Zhang Y, et al. Mater Charact. 2002;48:211-4.
[108] Yang D, Krasowska M, Priest C, Popescu MN, Ralston J. J Phys Chem C. 2011;115:18761-9.
[109] Zheng WJ, Wang LP, Or D, Lazouskaya V, Jin Y. Langmuir. 2012;28:12753-61.
[110] Kim TJ, Hidrovo C. Phys Fluids. 2012;24.
[111] de Gennes PG. Adv Colloid Interface Sci. 1987;27:189-209.
[112] Uhlmann P, Merlitz H, Sommer J, Stamm M. Macromol Rapid Comm. 2009;30:732-40.
[113] Rau ARP. J Biosci. 2002;27:475-8.
[114] Lauga E, Powers TR. Rep Prog Phys. 2009;72.
[115] Choi KS, Yang X, Clayton BR, Glover EJ, Atlar M, Semenov BN, et al. Proc R Soc London A. 1997;453:2229-40.
[116] McLean SC, Lioe H, Meagher L, Craig VSJ, Gee ML. Langmuir. 2005;21:2199-208.
[117] Lanotte L, Guido S, Misbah C, Peyla P, Bureau L. Langmuir. 2012;28:13758-64.
[118] Ng C-O, Wang CY. Fluid Dyn Res. 2011;43:065504.
[119] Ng C-O, Wang CY. Microfluid Nanofluid. 2010;8:361-71.
[120] Hendy SC, Lund NJ. Phys Rev E. 2007;76:066313.
[121] Davis AMJ, Lauga E. Phys Fluids. 2009;21:011701-4.
[122] Panzer P, Liu M, Einzel D. Int J Mod Phys B. 1992;6:3251-78.

[123] Kunert C, Harting J. Phys Rev Lett. 2007;99:176001.
[124] Ercolessi F. Spring College in Computational Physics, ICTP, Trieste. 1997;19.
[125] Jabbarzadeh A, Atkinson JD, Tanner RI. Phys Rev E. 2000;61:690-9.
[126] Galea TM, Attard P. Langmuir. 2004;20:3477-82.
[127] Priezjev NV, Troian SM. J Fluid Mech. 2006;554:25-46.
[128] Hoogerbrugge PJ, Koelman JMVA. Europhys Lett. 1992;19:155.
[129] Chen S, Doolen GD. Annu Rev Fluid Mech. 1998;30:329-64.
[130] Harting J, Kunert C, Hyväluoma J. Microfluid Nanofluid. 2010;8:1-10.
[131] Niavarani A, Priezjev NV. Phys Rev E. 2010;81:011606.
[132] Kunert C, Harting J. Int J Comput Fluid D. 2008;22:475-80.
[133] Gao J, Luedtke WD, Landman U. Tribol Lett. 2000;9:3-13.
[134] Lauga E, Stone HA. J Fluid Mech. 2003;489:55-77.
[135] Biben T, Joly L. Phys Rev Lett. 2008;100:186103.
[136] Mickel W, Joly L, Biben T. J Chem Phys. 2011;134:-.
[137] Hendy SC, Lund NJ. J Phys: Condens Matter. 2009;21:144202.
[138] Hyväluoma J, Kunert C, Harting J. J Phys: Condens Matter. 2011;23:184106.
[139] Cottin-Bizonne C, Barrat J-L, Bocquet L, Charlaix E. Nature Mater. 2003;2:237-40.
[140] Cottin-Bizonne C, Barentin C, Charlaix E, Bocquet L, Barrat J-L. Eur Phys J E. 2004;15:427-38.
[141] Ybert C, Barentin C, Cottin-Bizonne C, Joseph P, Bocquet L. Phys Fluids. 2007;19:123601.
[142] Jeon C, Jeong H, Jung Y. Phys Rev E. 2011;83:056324.
[143] Priezjev NV. J Chem Phys. 2011;135:204704.
[144] Hendy S, Jasperse M, Burnell J. Exploiting Stick and Slip in Nanofluidics. International Conference on Nanoscience and Nanotechnology 2006.
[145] Kuksenok O, Balazs AC. Phys Rev E. 2003;68:011502.
[146] Kuksenok O, Yeomans JM, Balazs AC. Langmuir. 2001;17:7186-90.
[147] Kuksenok O, Yeomans JM, Balazs AC. Phys Rev E. 2002;65:031502.
[148] Qian BT, Shen ZQ. Langmuir. 2005;21:9007-9.
[149] Priezjev NV, Darhuber AA, Troian SM. Phys Rev E. 2005;71:041608.
[150] Asmolov ES, Zhou J, Schmid F, Vinogradova OI. Phys Rev E. 2013;88:023004.
[151] Wang CY. Phys Fluids. 2003;15:1114-21.
[152] Asmolov ES, Schmieschek S, Harting J, Vinogradova OI. Phys Rev E. 2013;87:023005.
[153] Belyaev AV, Vinogradova OI. J Fluid Mech. 2010;652:489-99.
[154] Asmolov ES, Belyaev AV, Vinogradova OI. Phys Rev E. 2011;84:026330.
[155] Lee T, Hendy SC, Neto C. Macromolecules. 2012;45:6241–52.
[156] Adiga SP, Brenner DW. Nano Letters. 2005;5:2509-14.
[157] Binder K, Kreer T, Milchev A. Soft Matter. 2011;7:7159-72.
[158] Clément F, Charitat T, Johner A, Joanny JF. Europhys Lett. 2001;54:65.
[159] Dimitrov DI. J Chem Phys. 2007;127:084905.
[160] Dimitrov DI, Klushin LI, Milchev A, Binder K. Phys Fluids. 2008;20.
[161] Grest GS. Macromolecules. 1994;27:418-26.
[162] Huang J, Wang Y, Laradji M. Macromolecules. 2006;39:5546-54.
[163] Kim YW, Lobaskin V, Gutsche C, Kremer F, Pincus P, Netz RR. Macromolecules. 2009;42:3650-5.
[164] Kumaran V. Macromolecules. 1993;26:2464-9.
[165] Lai PY, Binder K. J Chem Phys. 1993;98:2366-75.
[166] Léonforte F, et al. J Phys: Condens Matter. 2011;23:184105.
[167] Miao L, Guo H, Zuckermann MJ. Macromolecules. 1996;29:2289-97.
[168] Milchev A, Dimitrov DI, Binder K. Biomicrofluidics. 2010;4.
[169] Milner ST. Macromolecules. 1991;24:3704-5.
[170] Müller M, Pastorino C. EPL. 2008;81:28002.
[171] Ouyang H, Xia Z, Zhe J. Microfluid Nanofluid. 2010;9:915–22.
[172] Peleg O, Tagliazucchi M, Kroeger M, Rabin Y, Szleifer I. ACS Nano. 2011;5:4737-47.
[173] Li N, Zuo C, Cao Q. J Macromol Sci B. 2011;51:275-87.
[174] Deng M, Li X, Liang H, Caswell B, Karniadakis GE. J Fluid Mech. 2012;711:192-211.
[175] Brinkman HC. Appl Sci Res. 1947;Al:27.
[176] Rabin Y, Alexander S. EPL. 1990;13:49.
[177] Wijmans CM, Smit B. Macromolecules. 2002;35:7138-48.
[178] Lim RYH, Deng J. ACS Nano. 2009;3:2911-8.
[179] Zhou F, Huck WTS. Phys Chem Chem Phys. 2006;8:3815-23.
[180] Lee T, Hendy SC, Neto C. Macromolecules. 2013;46:6326–35.
[181] Huh J, Ahn C-H, Jo WH, Bright JN, Williams DRM. Macromolecules. 2005;38:2974-80.
[182] Bechert DW, Bruse M, Hage W, Meyer R. Naturwissenschaften. 2000;87:157-71.
[183] Joly S, Ausserre D, Brotons G, Gallot Y. Eur Phys J E. 2002;8:355-63.

Graphical abstract